

# Deaminase-based RNA recording enables high throughput mutational profiling of protein-RNA interactions

Rachael A. Bakker<sup>1,2</sup>, Oliver B. Nicholson<sup>1</sup>, Heungwon Park<sup>1,2</sup>, Yu-Lan Xiao<sup>3</sup>, Weixin Tang<sup>3</sup>, Arvind Rasi Subramaniam<sup>1,2,†</sup>, and Christopher P. Lapointe<sup>1,†</sup>

<sup>1</sup> Basic Sciences Division, Fred Hutchinson Cancer Center, Seattle, WA 98109, USA,

<sup>2</sup> Computational Biology Section of the Public Health Sciences Division, Fred Hutchinson Cancer Center, Seattle, WA 98109, USA

<sup>3</sup> Department of Chemistry and Institute for Biophysical Dynamics, The University of Chicago, Chicago, IL 60637, USA

† Corresponding authors: A.R.S: [rasi@fredhutch.org](mailto:rasi@fredhutch.org), C.P.L. [cplapointe@fredhutch.org](mailto:cplapointe@fredhutch.org)

## 1 Abstract

2 Protein-RNA interactions govern nearly every aspect of RNA metabolism and are frequently dysregulated in  
3 disease. While individual protein residues and RNA nucleotides critical for these interactions have been charac-  
4 terized, scalable methods that jointly map protein- and RNA-level determinants remain limited. RNA deaminase  
5 fusions have emerged as a powerful strategy to identify transcriptome-wide targets of RNA-binding proteins by  
6 converting binding events into site-specific nucleotide edits. Here, we demonstrate that this ‘RNA recording’ ap-  
7 proach enables high-throughput mutational scanning of protein-RNA interfaces. Using the  $\lambda$ N-boxB system as  
8 a model, we show that editing by a fused TadA adenosine deaminase directly correlates with binding affinity be-  
9 tween protein and RNA variants *in vitro*. Systematic variation of RNA sequence context reveals a strong bias  
10 for editing at UA dinucleotides by the engineered TadA8.20, mirroring wild-type TadA preferences. We further  
11 demonstrate that stepwise recruitment of the deaminase using nanobody and protein A/G fusions maintains both  
12 sequence and binding specificity. Stable expression of the TadA fusion in human cells reproduces *in vitro* editing  
13 patterns across a library of RNA variants. Finally, comprehensive single amino acid mutagenesis of  $\lambda$ N in human  
14 cells reveals critical residues mediating RNA binding. Together, our results establish RNA recording as a versatile  
15 and scalable tool for dissecting protein-RNA interactions at nucleotide and residue resolution, both *in vitro* and in  
16 cells.

## 17 Introduction

18 RNA-binding proteins (RBPs) play a central role in post-transcriptional gene regulation. They control RNA  
19 processing, nuclear export, translation, stability, and subcellular localization. RBPs also mediate the assembly  
20 of larger ribonucleoprotein particles and granules, which play roles in diverse cellular functions. Dysregulated  
21 RBP-RNA interactions are implicated in a wide range of human diseases ([Gebauer et al. 2021](#)). A central goal,  
22 therefore, is to identify which RNAs are bound by which RBPs and reveal the molecular bases of the interactions.

23 Powerful approaches exist to examine RBP-RNA interactions *in vitro* and in cellular contexts, but they have  
24 limitations. For example, systematic evolution of ligands by exponential enrichment (SELEX), Bind-N-Seq, and  
25 SeqRS examine many thousands of RNA variants bound by an RBP *in vitro* ([Tuerk and Gold 1990](#); [Ellington  
26 and Szostak 1990](#); [Lambert et al. 2014](#); [Lou et al. 2017](#); [Becker et al. 2019](#); [Jarmoskaite et al. 2019](#)). These  
27 strategies define consensus binding motifs across a range of affinities, but they lack physiological context. They  
28 also only provide an RNA-centric perspective, as purification of hundreds or thousands of protein variants remains  
29 experimentally intractable. Cellular immunoprecipitation-based approaches (e.g., RIP-seq) capture snapshots of  
30 RBPs bound to RNAs in more native contexts, but they also may capture non-native interactions that form in  
31 lysates ([Zhao et al. 2010](#)). Crosslinking strategies, such as CLIP-seq and its many derivatives, circumvent this  
32 limitation and provide nucleotide-resolution views of RBP binding in cells ([Ule et al. 2005](#)). However, these

33 approaches are limited by crosslinking efficiency, antibody specificity, and biases introduced during crosslinking,  
34 RNA isolation, and sequencing. Thus, while current approaches have profoundly advanced our understanding of  
35 RBP-RNA interactions, it remains challenging to integrate *in vitro* mutational studies with *in vivo* profiling methods  
36 to achieve a more complete understanding of RBP function.

37 RNA recording-based approaches have emerged as a new strategy to uncover which RNAs are bound by  
38 an RBP in cells. In these approaches, an RBP of interest is fused to an RNA modification enzyme. The fusion  
39 protein covalently modifies bound RNAs, which can then be quantified by high-throughput sequencing. RNA  
40 modifying enzymes used for these studies include a poly(U) polymerase, engineered versions of the adenosine  
41 deaminase ADAR, and the cytosine deaminase APOBEC2 (Lapointe et al. 2015; McMahan et al. 2016; Rahman  
42 et al. 2018; Meyer 2019; Brannan et al. 2021). More recently, the *E. coli* adenosine deaminase TadA also has  
43 been engineered to enhance its efficiency and modify a broad range of RNA substrates (Xiao et al. 2023; Lin et al.  
44 2023). In each case, the resulting fusion proteins identified RNA targets of the RBP that significantly overlapped  
45 with ones identified using CLIP-based approaches. The editing marks accumulate in the RNAs over time, require  
46 less input material, and can be multiplexed using orthogonal enzymes. Thus, RNA recording provides a broader  
47 and complementary view of RBP-RNA interactions compared to direct binding-based approaches.

48 Given the success of RNA recording in identifying endogenous targets of RBPs, we sought to use this approach  
49 for mutational studies of protein-RNA interactions. We reasoned that the extent of editing (i.e., editing efficiency)  
50 should correlate with the affinity of an RBP or an RNA variant for its interaction partner. Since RNA editing can  
51 be carried out with purified enzymes or in cells, RNA recording can enable direct comparison of protein-RNA  
52 interactions between *in vitro* and cellular contexts. Further, expression of RBP variant libraries in cells could  
53 be used to study protein-RNA interactions from the protein perspective—a capability that current RNA-centric  
54 approaches lack. Here, we test the feasibility of these ideas using a model RBP-RNA system, and thereby  
55 demonstrate the utility of RNA recording to map the key molecular determinants of protein-RNA interactions at  
56 scale.

## 57 Results

### 58 Recruitment of a deaminase increases its editing efficiency on the RNA target.

59 We first tested whether fusing a deaminase to an RBP could direct its editing activity to a specific RNA target  
60 *in vitro*. As the editor, we used TadA8.20, an evolved variant of the *E. coli* TadA A-to-I deaminase (Wolf et al.  
61 2002). This enzyme has high activity and low sequence specificity on DNA (Gaudelli et al. 2020) and RNA  
62 (Xiao et al. 2023). As a model RBP, we selected the 22 amino acid  $\lambda$ N peptide that binds to a specific stem  
63 loop sequence called boxB (Chattopadhyay et al. 1995), and is widely used to tether proteins to RNAs for *in*  
64 *vivo* functional studies (De Gregorio et al. 1999; Baron-Benhamou et al. 2004). We purified TadA8.20 alone  
65 or as a TadA8.20- $\lambda$ N fusion protein (hereafter, TadA- $\lambda$ N) (Figure 1A). We incubated the purified proteins with a  
66 model reporter RNA engineered to contain or lack a boxB stem loop (Figure 1B). After incubation, reporter RNAs  
67 were reverse transcribed (RT), PCR-amplified, and analyzed by long read nanopore sequencing. A-to-I editing of  
68 RNA introduces A-to-G substitutions after RT-PCR, and hence the frequency of A-to-G substitutions in sequenced  
69 reads serves as a quantitative measure of editing efficiency (Figure 1B). TadA8.20 alone edited both reporters  
70 equally (50–60% editing efficiency, Figure 1C), consistent with its high and non-specific activity (Xiao et al. 2023).  
71 In contrast, TadA- $\lambda$ N showed significantly enhanced editing of the boxB-containing RNA (~90%) compared to  
72 the boxB-lacking control (40%) (Figure 1C). The increased editing with TadA- $\lambda$ N and boxB-containing RNA was  
73 evident in both single-edit or multi-edit analyses. These results demonstrate that recruitment of TadA- $\lambda$ N to boxB-  
74 containing RNA targets *in vitro* markedly increased editing efficiency.

## 75 **A high throughput editing assay for studying RNA-protein interactions.**

76 To enable mutational studies of RNA-RBP binding at scale, we developed a reporter assay with deep sequenc-  
77 ing readout of TadA-mediated RNA editing. Our RNA reporters consisted of a boxB stem loop and an A-rich  
78 ‘recorder’ region separated by an A-depleted spacer (Xiao et al. 2023) (Figure 2A). We *in vitro* transcribed the  
79 reporter and incubated the purified RNA with either the TadA- $\lambda$ N fusion or TadA8.20 alone. We performed the edit-  
80 ing reactions with the enzymes at excess (500nM), equimolar (250nM), or sub-saturating (125nM) concentrations  
81 relative to the RNA. After a 2 hour incubation and RT-PCR, we measured the frequency of A-to-G substitutions  
82 using Illumina short read sequencing. We examined the editing frequency of the A-rich recorder region and the  
83 boxB loop separately. Editing of the recorder region increased similarly at higher enzyme concentrations for both  
84 TadA- $\lambda$ N and TadA8.20 (Figure 2B, left). This observation is in line with the high non-specific editing efficiency  
85 of TadA8.20 (Xiao et al. 2023). However, while TadA8.20 on its own efficiently edited the adenosines within the  
86 boxB loop, TadA- $\lambda$ N editing of the boxB loop was reduced 2–5 fold relative to TadA8.20 at 250nM and 500nM con-  
87 centrations (Figure 2B, right). This observation is consistent with TadA- $\lambda$ N binding the boxB loop and protecting  
88 the adenosines within it from editing.

89 As a proof-of-principle pooled experiment, we examined whether the distance between and orientation of the  
90 boxB stem loop and the recorder region affected editing efficiency of the reporter. We synthesized a pooled RNA  
91 library with varying distances (0–30nt) between the boxB stem loop and the recorder region in either 5’ and 3’  
92 orientations (Figure 2C, top). We incubated the library with TadA- $\lambda$ N and sequenced the edited regions as above.  
93 TadA- $\lambda$ N edited recorder regions at various distances from boxB at similar efficiencies (Figure 2C). This lack of  
94 distance and orientation preference might arise from the long flexible linker (96aa) between the  $\lambda$ N and TadA  
95 domains in our construct. Thus, for all subsequent pooled library experiments, we included both recorder region  
96 orientations and combined the data for analyses.

## 97 **TadA8.20 editing is sensitive to the sequence context of the edited adenosine.**

98 TadA8.20 was evolved from a natural *E. coli* enzyme that edits the adenosine within a UAC loop in a specific  
99 tRNA (Wolf et al. 2002). Since engineered TadA enzymes also exhibit editing preference towards adenosines  
100 adjacent to pyrimidines (T or C) on DNA (Gaudelli et al. 2020; Xiao et al. 2024b), we examined whether Tad8.20  
101 might exhibit sequence context preferences during RNA editing. We analyzed editing across the 8 adenosines  
102 of the recorder region in our reporters, each of which has a unique combination of 5’ and 3’ flanking bases. The  
103 UAG and UAC contexts had the highest editing rates, at 17.5 % and 11.6 % respectively (Figure 2D), with the  
104 latter context the same as the tRNA sequence context of the natural TadA enzyme. The six other adenosines  
105 in our recorder region had 2- to 10-fold lower editing efficiency relative to UAG. We observed these differences  
106 between adenosine contexts at all concentrations of TadA- $\lambda$ N tested (Supplementary Figure 1A).

107 To assess the apparent sequence bias of TadA8.20 more systematically, we designed a library with random-  
108 ized sequence contexts around the eight adenosines in the recorder region of our reporter (Figure 2A). This  
109 randomization yielded four adenosines with all possible combinations of 5’ and 3’ flanking nucleotides, and four  
110 other adenosines with only the 5’ or the 3’ flanking nucleotide varied. For analyzing the results, we combined  
111 flanking adenosines and guanosines into a single purine base ‘R’, since edited adenosines are indistinguishable  
112 from unmodified guanosines. Consistent with our analysis of the unmodified recorder region, all adenosines with  
113 a 5’ uridine were edited at 5- to 10-fold higher rates than other sequence combinations (Figure 2E, Supplementary  
114 Figure 1B). Presence of a 3’ U (UAU context) further enhanced editing by 1.5–2 fold, and resulted in the highest  
115 editing efficiency across all flanking contexts at 24–45%. Conversely, the CAC or CAR flanking contexts had the  
116 lowest editing efficiency at 1–2%. Together, our analyses show that TadA8.20, despite its high editing efficiency  
117 on RNA, retains its native specificity for UA dinucleotide motifs (Wolf et al. 2002).

118 We also compared our *in vitro* results to another TadA-derived RNA base editor, rABE, that was recently

119 used to identify RBP binding sites *in vivo* (Lin et al. 2023). In that published data, we found that the TadA7.10-  
120 derived rABE base editor had higher editing efficiency when the edited adenosine was flanked by a 5' U or C  
121 (Supplementary Figure 1C). This observation on native RNAs is consistent with TadA7.10's preference on DNA  
122 (Xiao et al. 2024b). By contrast, our findings demonstrate that TadA8.20 exhibits a preference for only UA,  
123 suggesting that the two enzyme variants have distinct sequence preferences on RNA.

#### 124 **TadA- $\lambda$ N editing quantitatively reflects RNA-RBP binding strength *in vitro*.**

125 *In vivo* expression of deaminase-RBP fusions yields variable editing efficiencies across endogenous RNAs  
126 (Medina-Munoz et al. 2024). However, because endogenous RNAs differ in sequence, structure, and associated  
127 RBPs, it is unclear whether editing efficiency reliably reflects RBP binding strength. To directly test this relationship,  
128 we used our *in vitro* system to measure editing across defined RNA libraries with controlled sequence variation.  
129 We designed reporter libraries in which the boxB stem and loop regions were randomized in 3nt or 4nt windows,  
130 while the recorder region remained constant (Figure 3A,H; Supplementary Table 1). We incubated these libraries  
131 with either sub-saturating or saturating concentrations of TadA- $\lambda$ N for varying durations, and quantified the average  
132 A-to-G substitution frequency for each boxB variant.

133 Editing by  $\lambda$ N-TadA recapitulated several known features required for  $\lambda$ N binding to boxB (Figure 3B-H). Prior  
134 structural and biochemical analyses showed that  $\lambda$ N preferentially binds a GNRNA pentaloop (N=A/C/G/U, R=A/G)  
135 (Legault et al. 1998). This sequence forms a GNRA tetraloop (with the second N extruded), a common RNA fold  
136 recognized by many RBPs (Thapar et al. 2014). Consistently, boxB variants containing a GNRNA motif in its  
137 loop were edited more efficiently by TadA- $\lambda$ N than those without under sub-saturating enzyme concentrations  
138 (median editing: 15 vs 10%,  $p=3.5e-13$ ) (Figure 3B). The GAAGA motif from wild-type boxB ranked among the  
139 highest-edited sequences (30.1%, Figure 3B). Interestingly, a non-canonical variant (UGAGA) was also highly  
140 edited (Figure 3B), suggesting that  $\lambda$ N can tolerate alternative sequence registers in boxB that may adopt similar  
141 RNA folds. Further analysis revealed that guanosine at position 8 and a purine at position 10—core components  
142 of the GNRNA motif—were associated with the highest editing levels (Figure 3C). These findings agree with prior  
143 evidence that G8 and A10 are required for high-affinity  $\lambda$ N binding and transcriptional regulation (Chattopadhyay  
144 et al. 1995; Tan and Frankel 1995). Position 12 is part of the GNRNA tetraloop, but it does not directly contact  
145  $\lambda$ N residues in structures of the  $\lambda$ N-boxB complex (Legault et al. 1998; Schärpf et al. 2000). An A in position  
146 12 yielded moderately higher editing ( $\sim 0.8$ -fold) when position 10 was G, and showed a preference for R when  
147 position 10 was a pyrimidine (Figure 3D). This is consistent with position 12 playing a secondary role in  $\lambda$ N  
148 recognition of boxB, likely by stabilizing the tetraloop structure. These results reinforce the importance of GNRA-  
149 like motifs for  $\lambda$ N binding to boxB.

150 In addition to the loop,  $\lambda$ N requires the closing U7-A13 basepair of the stem for high-affinity binding (Tan and  
151 Frankel 1995). Variants preserving this base pair exhibited higher editing rates than mismatched pairs (Figures  
152 3E,F). Uridine at position 7—known to make direct contacts with  $\lambda$ N in structures (Schärpf et al. 2000)—was strongly  
153 enriched for higher editing (Figure 3G). In contrast, adenosine at position 13 was only weakly favored, and all  
154 four nucleotides supported relatively high levels of editing (Figure 3F). These observations suggest that U7 is  
155 the key determinant, while base pairing at this position contributes less. At saturating concentration of TadA- $\lambda$ N,  
156 enrichment for U7 and the GNRNA-like motifs diminished, suggesting increased non-specific editing, as expected  
157 (Supplementary Figure 2A). Consistently, TadA8.20 alone did not reproduce these features for high-affinity  $\lambda$ N  
158 binding (Supplementary Figure 2B).

159 Editing efficiency also strongly correlated with the thermodynamic stability of the boxB stem. We used RNAfold  
160 (Lorenz et al. 2011) to calculate the predicted free energy ( $\Delta G$ ) of each stem variant in our libraries (Figure  
161 3I), and grouped them into bins from most to least stable. On average, TadA- $\lambda$ N more efficiently edited boxB  
162 variants predicted to have more stable boxB stems than those with less stable stems (Figure 3J). This trend  
163 was evident across timepoints, with editing efficiency increasing over time. While diminished relative to TadA- $\lambda$ N,

164 TadA8.20 alone also showed modestly higher editing for the most stable stem variants (Supplementary Figure  
165 2C, bottom), suggesting that TadA8.20 itself may bind RNA hairpins at low levels, contributing to off-target effects.  
166 Increasing the concentration of TadA- $\lambda$ N or TadA8.20 to a saturating level also decreased the correlation between  
167 editing efficiency and apparent stem stability, consistent with the expected shift to a non-specific binding regime  
168 (Supplementary Figure 2C, right). Together, these results demonstrate that TadA- $\lambda$ N editing quantitatively reflects  
169 RNA-RBP binding strength *in vitro*, capturing both sequence and structural determinants of high-affinity  $\lambda$ N-boxB  
170 recognition.

### 171 **Split recruitment preserve RNA editing specificity.**

172 In addition to direct fusion of RBPs to RNA-modifying enzymes, recent studies have used nanobody and  
173 protein A/G fusions to recruit RNA editors and reverse transcriptases to RBPs (Liang et al. 2024; Xiao et al.  
174 2024a; Khyzha et al. 2022). These “split” strategies eliminate the need to generate deaminase fusions for each  
175 RBP, enabling broader application to fixed cell lines and tissues. However, it remains unclear how the efficiencies  
176 and specificities of split recruitment approaches compare to those of the direct fusion approach. To address this  
177 question, we examined two split recruitment strategies using a nanobody or protein A/G (pAG) to recruit TadA8.20  
178 to boxB-containing RNAs. To enable direct comparison, we purified  $\lambda$ N-GFP and used either a purified TadA8.20-  
179 GFP nanobody fusion (henceforth TadA-GFPnb) or a monoclonal anti-GFP antibody in combination with purified  
180 pAG-TadA8.20 (henceforth pAG-TadA) (Figure 4A,B, Supplementary Figure 3A).

181 Reporter mRNAs with or without a boxB stem loop were incubated with  $\lambda$ N-GFP and either TadA-GFPnb or the  
182 anti-GFP primary antibody and pAG-TadA proteins, followed by RT-PCR and nanopore sequencing. Incubation  
183 with TadA-GFPnb or pAG-TadA alone (without  $\lambda$ N-GFP or anti-GFP antibody present) edited both reporter mRNAs  
184 regardless of boxB sequence (Figure 4B), similar to background editing observed with the direct TadA- $\lambda$ N fusion.  
185 By contrast, addition of  $\lambda$ N-GFP yielded a 2–4 fold increase in editing of the boxB-containing mRNA relative to  
186 boxB-lacking mRNA in both split recruitment strategies (Figure 4B). Using our high-throughput reporter assay,  
187 we found that both split recruitment strategies produced robust editing in the recorder region, whereas the boxB  
188 loop sequence was edited at a lower frequency (Figure 4C). Both TadA-GFPnb and pAG-TadA retained their  
189 preference for UA dinucleotides in the recorder region (Supplementary Figure 3B). Together, these results show  
190 that both split recruitment strategies recapitulate the editing specificity of the direct TadA- $\lambda$ N fusion.

191 We tested the split recruitment strategies on the boxB loop- and stem-randomized libraries to determine if  
192 they recover sequence and structural preferences of  $\lambda$ N binding. Both split strategies yielded higher editing  
193 when recruited by GNRNA boxB loops relative to non-GNRNA loops (Figure 4D). However, several non-GNRNA  
194 loops exhibited comparable editing to GNRNA loops when recruiting pAG-TadA. This finding suggests that the  
195 increased complexity of this strategy, requiring successful formation of a four component complex, may reduce  
196 specificity. Nevertheless, both split strategies showed higher editing when recruited by loop variants with a G in  
197 position 8, a purine in position 10, and a uridine in position 7 (Figure 4E), while position 12 had minimal influence  
198 (Supplementary Figure 3C). Editing efficiency of both approaches also correlated with the predicted stability of the  
199 boxB stems (Figure 4F). Finally, the extent of editing by TadA-GFPnb or pAG-TadA significantly correlated with  
200 that of TadA- $\lambda$ N, but diverged from that of TadA8.20 alone (Supplementary Figure 3D-E). Together, these results  
201 show that the two split recruitment strategies preserve key hallmarks of high-affinity binding by  $\lambda$ N, but can result  
202 in higher non-specific editing than the direct fusion approach in certain contexts.

### 203 ***In vivo* analysis of TadA- $\lambda$ N recruitment and editing**

204 We next asked whether editing patterns observed *in vitro* with purified enzymes are preserved when the  
205 same constructs are expressed *in vivo* in human cells. We focused on editing by TadA- $\lambda$ N and TadA-GFPnb  
206 for our *in vivo* experiments, as pAG-TadA requires antibody binding and is not readily applicable to living cells.  
207 We designed a reporter library consisting of either EGFP or  $\lambda$ N-EGFP mRNA with a boxB stem loop and an

208 A-rich recorder region in the 3' UTR (Figure 5A). The boxB stem loop was randomized in 3- or 4-nucleotide  
209 increments similar to our previous *in vitro* stem loop libraries. We co-expressed the EGFP and  $\lambda$ N-EGFP reporter  
210 libraries with either TadA- $\lambda$ N or TadA-GFPnb, with both the reporter and the TadA constructs under the control  
211 of a doxycycline-inducible promoter. We integrated the libraries into the *AAVS1* locus of HEK293T cells using  
212 site-specific Bxb1-mediated integration (Nugent et al. 2024), ensuring that each cell expressed a single boxB  
213 variant in combination with either TadA- $\lambda$ N or TadA-GFPnb. We also generated a control cell line expressing only  
214 the EGFP reporter, without a TadA construct. After doxycycline induction for 72 hours, we harvested RNA and  
215 analyzed editing efficiency by deep sequencing the 3' UTR of the reporter (Figure 5A).

216 Cells expressing TadA- $\lambda$ N or TadA-GFPnb showed increased editing in the recorder region compared to control  
217 cells not expressing TadA (15% vs 0.3% reads with 1 or more edit, Figure 5B). We observed higher editing in  
218 the UAG, UAC, and UAA sequence contexts relative to the other trinucleotide contexts in the recorder region  
219 (Figure 5C), mirroring our *in vitro* observations. Editing rates were lower *in vivo* than *in vitro* at all concentrations,  
220 presumably due to limiting *in vivo* enzyme levels arising from single copy integration. Editing rates for different  
221 boxB variants were correlated between the direct fusion and split recruitment strategies *in vivo* ( $R=0.5$ ) (Figure  
222 5D). Notably, the *in vivo* editing rates of the boxB variants were also significantly correlated with the *in vitro* editing  
223 rates (Figure 5E). The *in vivo* correlation was slightly stronger for the direct fusion than for split recruitment ( $R=0.53$   
224 vs  $R=0.5$ ), presumably reflecting the more complex requirement in the latter case for two proteins and the RNA  
225 reporter to bind together in the crowded cellular environment. For both the direct fusion and the split recruitment  
226 strategies, GNRNA boxB loop variants resulted in significantly higher editing rates than non-GNRNA variants  
227 (Figure 5F), confirming that TadA- $\lambda$ N binding specificity observed *in vitro* persists in cells. Given the overall  
228 lower levels of editing, comparisons of base combinations at different positions were noisy, though we observed  
229 consistently elevated editing levels for guanosine at positions 8, 10 and 12 (Supplementary Figure 4A and B).  
230 While differences in editing based on stem stability were less pronounced in the cellular context compared to *in*  
231 *vitro* results, stronger hairpins still exhibited higher editing rates, with the strongest hairpins showing a significantly  
232 elevated editing (Figure 5G). RNA secondary structures are subject to additional layers of regulation in a cellular  
233 context due to interactions with intracellular RBPs (Georgakopoulos-Soares et al. 2022), which may explain  
234 why calculated free energy is less predictive of  $\lambda$ N binding-mediated RNA editing. In summary, TadA- $\lambda$ N editing  
235 patterns in cells recapitulate our *in vitro* results, albeit with reduced resolution across boxB variants and overall  
236 lower editing levels.

### 237 **Deep mutational scanning of the $\lambda$ N RNA-binding domain**

238 Since the above *in vivo* experiments resolved affinity differences between an invariant  $\lambda$ N and boxB RNA  
239 variants, we next asked whether RNA editing can also be used to study interactions between a fixed boxB stemloop  
240 and  $\lambda$ N peptide variants. Such a high-throughput approach would complement existing methods that probe RNA  
241 variant libraries against fixed RBPs (Tuerk and Gold 1990; Ellington and Szostak 1990; Lambert et al. 2014; Lou  
242 et al. 2017). To this end, we constructed a comprehensive single-codon substitution library by randomizing all  
243 22 codons of the  $\lambda$ N open reading frame, yielding 1,408 ( $22 \times 64$ ) unique variants. We expressed this  $\lambda$ N variant  
244 library as a fusion with TadA8.20 and co-expressed it with an mRNA reporter containing a boxB stem loop and  
245 an A-rich recorder region in the 3' UTR (Figure 6A). Both the TadA- $\lambda$ N and reporter expression cassettes were  
246 under the control of a doxycycline-inducible promoter as in our previous *in vivo* experiment. We included a random  
247 20-nucleotide A-depleted barcode upstream of the recorder region during cloning, allowing each  $\lambda$ N codon variant  
248 to be uniquely linked to a median of 8 barcodes, as confirmed by deep sequencing (Supplementary Figure 5A).  
249 We integrated the libraries into the *AAVS1* locus of HEK293T cells using site-specific Bxb1-mediated integration  
250 (Nugent et al. 2024), ensuring that each cell expressed a single  $\lambda$ N codon variant. After 72 hours of doxycycline  
251 induction, we harvested RNA and deep sequenced the 3'UTR to measure editing efficiency in the recorder region,  
252 and assigned each read to a  $\lambda$ N variant via its associated barcode.

253 While the editing efficiency by individual  $\lambda$ N amino acid variants was noisy (Supplementary Figure 5A), several  
254 biologically meaningful patterns emerged (Figure 6B). First, mutations introducing premature stop codons resulted  
255 in the largest decrease in editing efficiency, consistent with disruption of  $\lambda$ N–boxB binding by truncated peptides  
256 (Figure 6B). Second, nearly all substitutions of wild-type arginine codons at positions 6, 7, 8, 10, and 11 led  
257 to substantial reductions in editing (Figure 6B). Comparison with an existing NMR structure for the  $\lambda$ N–boxB  
258 complex (Schärpf et al. 2000) revealed that these positions map to the face of the  $\alpha$ -helix that directly contacts  
259 the boxB hairpin (Figure 6C). This is consistent with previous biochemical studies showing that the arginine-rich  
260  $\alpha$ -helical motif of  $\lambda$ N is essential for both boxB recognition and helix stabilization (Chattopadhyay et al. 1995;  
261 Tan and Frankel 1995). In particular, Arg7 and Arg11—both of which make close contacts with nucleotide U7 of  
262 boxB—exhibited the lowest mean editing efficiencies (Figure 6C, right panel). Glu9 was the only residue within the  
263 arginine-rich motif whose mutation had minimal effect on editing efficiency, consistent with its orientation away from  
264 the RNA interface and lack of direct contacts with boxB. Substitutions at Lys14 also reduced editing in many cases,  
265 likely reflecting its proximity to the RNA backbone (Figure 6C, right panel). Together, these results show that *in*  
266 *vivo* RNA recording can be effectively combined with deep mutational scanning to identify amino acid residues in  
267 RBPs that are critical for RNA recognition and binding.

## 268 Discussion

269 Here, we present a high-throughput strategy to interrogate the molecular interactions that underlie protein–  
270 RNA binding. Our RNA recording strategy leverages an RNA editing approach commonly used to map  
271 transcriptome-wide RBP binding sites. We adapt this system to comprehensively assess the effects of amino  
272 acid and nucleotide mutations on RBP–RNA interactions. We find that deamination by an RNA editor fused to  
273 an RBP captures changes in RNA–RBP interactions both *in vitro* and in cells. We show that this strategy, which  
274 relies on high throughput DNA sequencing to measure RNA editing, can be applied across diverse libraries of  
275 sequence variants, with mutations introduced on either the RNA or the protein side.

276 Our RNA recording system used an engineered adenosine deaminase, TadA8.20, derived from a natural  
277 tRNA deaminase from *E. coli*. (Wolf et al. 2002) Given its high activity on nucleic acid substrates, TadA8.20 is well  
278 suited for RNA recording applications (Gaudelli et al. 2020). Indeed, we confirmed that TadA8.20 deaminates  
279 adenosines in a variety of sequence contexts both *in vitro* and in cells. However, by systematically varying the  
280 adenosine context, we find that TadA8.20 partly retains the substrate specificity of its tRNA-deaminating ancestor,  
281 which targets A34 flanked by U33 and C35 in the anticodon loop of a tRNA (Wolf et al. 2002). Specifically, the  
282 identity of the nucleotide immediately preceding the adenosine strongly impacted the editing efficiency. TadA8.20  
283 preferentially deaminated UA dinucleotides, with up to 10-fold higher activity than for other dinucleotide motifs.  
284 We also found that the rABE editor—a distinct TadA variant with two substitutions relative to TadA8.20—exhibits  
285 similar but distinct preferences, favoring UA and CA motifs in cells (Lin et al. 2023). Thus, recent efforts (Xiao et  
286 al. 2024b) to broaden the editing context of TadA by reducing its DNA specificity may further improve its utility for  
287 RNA recording applications.

288 Our RNA recording strategy captured several key determinants of high-affinity binding between the RNA-  
289 binding domain of  $\lambda$ N and its cognate boxB RNA target. Using libraries of boxB RNA variants, we found that  
290 substitution of U7—which pairs with A13 to close the boxB stem—and G8—the first nucleotide of the boxB loop—  
291 led to the largest decreases in editing efficiency *in vitro* and in human cells. Consistently, both nucleotides make  
292 direct contacts with  $\lambda$ N in structures of the complex (Legault et al. 1998; Schärpf et al. 2000). Substitution of three  
293 other nucleotides within the loop (A9, G11, A12) and A13 of the closing base pair had intermediate or minimal  
294 effects in our assays. These bases lack direct contacts with  $\lambda$ N in the structure (Legault et al. 1998; Schärpf et al.  
295 2000). Conversely, substitution of A10, the third loop position, to guanosine had little effect, while substitution to a  
296 pyrimidine dramatically impaired  $\lambda$ N binding. This position forms the purine core of the GNRNA tetraloop required  
297 for the boxB hairpin to adopt its functional conformation. From the protein side, our deep mutational scanning

of >400  $\lambda$ N variants identified the arginine-rich patch spanning residues 6–11 as most critical for RNA editing in human cells. Conversely, substitution of Glu9, an internal residue surrounded by the arginine patch, was largely inert, consistent with its lack of direct RNA contacts and prior studies. Thus, RNA recording can pinpoint individual nucleotide or amino acid residues that are essential or dispensable for an RBP-RNA interaction.

While we demonstrated our approach using the  $\lambda$ N–boxB system, RNA recording could be extended to a wide range of RBPs and biological contexts. Prior *in vivo* strategies to map protein–RNA interactions or mutation effects often relied on genetic, transcriptional, or reporter-based readouts (SenGupta et al. 1996; Melamed et al. 2013). By using RNA edits as a molecular proxy of binding, RNA recording enables more direct and scalable mutational dissection of RBP–RNA interactions in human cells. Furthermore, we show that TadA8.20 recruitment via direct fusion, nanobody-based tethering, or antibody-pA/G tethering discriminates between high- and low-affinity binding events. This flexibility will enable adaptation of the method to purified systems, live cells, or fixed tissues. However, our findings also highlight trade-offs: increased complexity in recruitment strategies can reduce editing efficiency and resolution. Optimizing the ratios and delivery of each component may be especially important in complex or heterogeneous biological samples. Nonetheless, our work establishes RNA recording with deaminase fusions as a versatile, high throughput platform for identifying the molecular determinants of protein–RNA interaction.

### Author Contributions

R.A.B. designed research, performed experiments, analyzed data, and wrote the manuscript. H.P. and O.N. performed experiments. Y.X. and W.T. contributed reagents and technical expertise. A.R.S. and C.P.L. designed research, analyzed data, wrote the manuscript, supervised the project, and acquired funding.

### Acknowledgements

We thank members of the Subramaniam and Lapointe labs, the Basic Sciences Division, and the Computational Biology Program at Fred Hutch for assistance with the project and discussions and feedback on the manuscript. We thank Tao Pan for initial discussions on using TadA8.20 for RNA recording. This research was funded by NIH R35 GM119835 (A.R.S.), NSF MCB 1846521 (A.R.S.), NSF PRFB 2209388 (R.A.B.), NIH R00 GM144678 (C.P.L.), and the Damon Runyon Cancer Research Foundation (DFS-49-22 to C.P.L.). This research was supported by the Genomics, Flow Cytometry, and Proteomics Shared Resources of the Fred Hutch/University of Washington Cancer Consortium (P30 CA015704) and Fred Hutch Scientific Computing (NIH grants S10-OD-020069 and S10-OD-028685). The funders had no role in study design, data collection and analysis, decision to publish, or preparation of the manuscript.

### Competing interests

None

### Data and Code Availability

All high-throughput sequencing data generated in this study are available at the NCBI Sequence Read Archive (SRA) under BioProject PRJNA1255650. All other data and programming code associated with this manuscript are publicly available at [https://github.com/rasilab/bakker\\_2025](https://github.com/rasilab/bakker_2025).

### Materials and Methods

Plasmids, oligonucleotides, and cell lines used in this study are listed in supplemental tables S1-S3. DNA sequences of plasmids used in this study are available at [https://github.com/rasilab/bakker\\_2025/](https://github.com/rasilab/bakker_2025/). Information not included below can be requested at [https://github.com/rasilab/bakker\\_2025/issues/](https://github.com/rasilab/bakker_2025/issues/).

## 337 Plasmid construction

338 **Protein expression plasmids:** The parent TadA8.20 expression plasmid in a pET28a backbone was de-  
339 scribed previously (Xiao et al. 2023). To generate TadA-GFPNb expression vector (pAS95), Gibson assembly  
340 was performed using this plasmid as a backbone along with the following components: a His14x-Avi-SumoEu1  
341 fragment (amplified with primers oRB96 and oRB97), a 48-amino-acid extended XTEN linker (Yarnall et al. 2023),  
342 and the GFPNb sequence. This vector (pAS95) served as the template for constructing additional protein expres-  
343 sion plasmids.

344 To generate the TadA- $\lambda$ N expression plasmid (pAS335), pAS95 was digested with BamHI and XhoI to remove  
345 the GFPNb insert. The resulting backbone was assembled via Gibson with a synthetic  $\lambda$ N fragment (oAS2160,  
346 ordered from GenScript).

347 To construct the pAG-TadA expression plasmid (pAS428), pAS95 was digested with XhoI and SacI to remove  
348 the XTEN-GFPNb region. The backbone was assembled with the pAG sequence (amplified from the pAG/MNase  
349 plasmid, Addgene #123461, using primers oRB226, oRB227, and oRB228; a gift from the Henikoff lab) and a  
350 pAG-specific linker (amplified from pAG/MNase using primers oRB231 and oRB242).

351 To generate the  $\lambda$ N-EGFP expression plasmid, pAS95 was digested with BamHI and XhoI to remove the  
352 TadA-GFPNb insert. The resulting backbone was assembled with a synthetic  $\lambda$ N fragment (oAS2159, ordered  
353 from GenScript) and an EGFP-containing sequence.

354 **Reporter libraries for *in vivo* expression:** First, TadA-GFPNb and TadA- $\lambda$ N coding sequences were ampli-  
355 fied from their respective expression plasmids using primers oRB245/oRB246 and oRB247/oRB248, respectively.  
356 These fragments were cloned using Gibson assembly into a backbone vector containing a cHS4 insulator se-  
357 quence and pTet Doxycycline inducible promoter sequence. These plasmids were pAS440 (TadA-GFPNb) and  
358 pAS441 (TadA- $\lambda$ N).

359 Next, the resulting plasmids were digested with *MluI* and *AgeI*, and new constructs were assembled using  
360 a fragment containing the rbGlobin\_pA polyadenylation signal, a pTet promoter, and either the EGFP or  $\lambda$ N-  
361 EGFP coding sequence (amplified with ) to create pAS443 (TadA-GFPNb +  $\lambda$ N-EGFP) and pAS444 (TadA- $\lambda$ N  
362 + EGFP). These promoter-EGFP plasmids were then digested with *NotI* and ligated into EcoRV-digested parent  
363 vectors (pAS457) containing attB sequences for Bxb1 recombinase integration into the genome, mCherry, and  
364 puromycin resistance as markers for integration. The resulting intermediate vectors were pAS472(TadA-GFPNb)  
365 and pAS473 (TadA- $\lambda$ N). Following this, these intermediate vectors were digested with *NotI*, and the boxB re-  
366 porter library oligo pool (oRB262) was inserted via Gibson assembly to create pAS475 (TadA-eGFP) and pAS476  
367 (TadA- $\lambda$ N). The resulting library was cloned with >300,000 colonies to retain library complexity.

368 To construct the  $\lambda$ N site saturation mutagenesis library, the parent vector pAS457 was digested with  
369 *MluI* and *SpeI* to remove the TadA- $\lambda$ N insert. This was replaced with a TadA-XTEN fragment (amplified  
370 with oRB276/oRB283) via Gibson assembly. In parallel, the boxB reporter sequence was amplified with  
371 oRB268/oRB269 and cloned into a separate plasmid bearing the attB site using the NEBuilder HiFi DNA  
372 Assembly system (NEB). These two intermediate plasmids were then digested with *NotI* and EcoRV, respectively,  
373 and assembled via Gibson to generate pAS496.

374 The  $\lambda$ N site saturation mutagenesis library was synthesized as an oligo pool (oRB275) by IDT. This pool was  
375 amplified using primers oRB271 and oRB284 to append a unique 20-nt DNA barcode and homology arms for  
376 Gibson assembly. The plasmid pAS496 was digested with *AgeI* and *MluI*, and the barcoded  $\lambda$ N mutagenesis  
377 library was inserted in-frame with the upstream TadA-XTEN via Gibson assembly. The final transformants were  
378 bottlenecked to 17,500 colonies, providing >10 $\times$  coverage of the 1,408  $\lambda$ N variants in the library. The resulting  
379 plasmid pool (pAS499) was sequenced to link each 20-nt barcode to its corresponding  $\lambda$ N variant.

380 To complete the functional reporter construct, pAS499 was digested with *MluI*, and a fragment containing the

381 rbGlobin terminator, pTet promoter, and EGFP coding sequence (from pAS444 digested with AgeI and MluI) was  
382 inserted via Gibson assembly. This positioned the barcode and boxB reporter within the 3' UTR of EGFP. The  
383 final library was cloned with >2 million colonies to maintain high representation of  $\lambda$ N variants and barcodes. The  
384 resulting plasmid pool (pAS517) was used for genomic integration into cell lines.

### 385 Protein purification

386  **$\lambda$ N-EGFP:** The plasmid was transformed into Rosetta 2 cells purchased from the UC Berkeley QB3 MacroLab  
387 and grown overnight at 37 °C on LB agar plates supplemented with 50  $\mu$ g/mL of kanamycin. Liquid cultures of  
388 single colonies were grown at 37 °C in LB supplemented with kanamycin. At an OD<sub>600</sub> of 0.5, isopropyl  $\beta$ -D-1-  
389 thiogalactopyranoside (IPTG) was added at a final concentration of 0.5 mM. After two hours at 37 °C, the cultures  
390 were shifted to 16 °C and grown overnight. Cells were harvested by centrifugation at 5,000 x g for 10 minutes  
391 at 4 °C in a Fiberlite F9 rotor (ThermoFisher, cat # 096-061075). Cells were lysed by sonication in lysis buffer  
392 (20 mM Tris-HCl pH 8.0, 300 mM NaCl, 10% (v/v) glycerol, 30 mM imidazole, and 5 mM  $\beta$ -mercaptoethanol)  
393 supplemented with protease inhibitors (ThermoFisher, cat # A32965). Lysates were cleared by centrifugation at  
394 27,000 x g for 45 minutes at 4 °C in a Sorvall SS-34 rotor. Clarified lysate was loaded onto Ni-NTA resin (Qiagen,  
395 cat # 30210) equilibrated in lysis buffer in a gravity flow column. The resin was then washed with 10 column  
396 volumes (CV) of lysis buffer, 10 CV of wash buffer (20 mM Tris-HCl pH 8.0, 1000 mM NaCl, 10% (v/v) glycerol,  
397 30 mM imidazole, and 5 mM  $\beta$ -mercaptoethanol), and 10 CV of lysis buffer. Recombinant protein was eluted in  
398 five CV of elution buffer (20 mM Tris-HCl pH 8.0, 300 mM NaCl, 10% (v/v) glycerol, 300 mM imidazole, and 5  
399 mM  $\beta$ -mercaptoethanol). Fractions with recombinant protein were identified by SDS-PAGE analysis. Relevant  
400 fractions were dialyzed overnight at 4 °C into dialysis buffer (20 mM Tris Ph 8.0, 250 mM NaCl, 10% (v/v) glycerol,  
401 and 5 mM  $\beta$ -mercaptoethanol) in the presence of TEV protease. TEV protease and the cleaved 14xHis-SUMO-  
402 Avi tag were captured via a subtractive Ni-NTA gravity column equilibrated in dialysis buffer supplemented with  
403 30 mM imidazole. The flowthrough was collected and concentrated to 500  $\mu$ L with a 10k MWCO concentrator  
404 (MilliporeSigma, cat # UFC901096) then applied to a 23 mL Superdex 200 Increase 10/300 GL SEC column  
405 (Cytiva, cat # 28990944). Fractions that contained purified  $\lambda$ N-EGFP were concentrated, frozen in liquid N<sub>2</sub>, and  
406 stored at -80 °C.

407 **TadA-GFPnb:** Protein was purified as described above with the following modifications. Following the sub-  
408 tractive Ni-NTA step, the protein was diluted to 75 mM NaCl using 20 mM Tris-HCl pH 7.5 and applied to a 1 mL  
409 heparin column (Cytiva, cat # 17040601). Purified protein was eluted using a 50 to 1000 mM NaCl gradient in the  
410 absence of reducing agents. Fractions that contained purified  $\lambda$ N-EGFP were concentrated, frozen in liquid N<sub>2</sub>,  
411 and stored at -80 °C.

412 **TadA- $\lambda$ N:** Protein was purified as described above for TadA-GFPnb.

413 **pAG-TadA-ybbR:** Protein was purified as described above for TadA-GFPnb. Fractions with recombinant pro-  
414 tein from the 1 mL heparin column were collected, concentrated, and further purified using a SD200 120 mL SEC  
415 column (Cytiva, cat # 28989335). Fractions that contained purified  $\lambda$ N-eGFP were concentrated, frozen in liquid  
416 N<sub>2</sub>, and stored at -80 °C.

417 **TadA:** Protein was purified as described above for TadA-GFPnb.

418 The identity of purified proteins was confirmed using standard mass spectrometry analyses in the Proteomics  
419 and Metabolomics Shared Resource at Fred Hutch.

### 420 Antibody

421 GFP antibody (HtzGFP-19F7) was acquired from the Memorial Sloan Kettering Cancer Center.

## 422 ***In vitro* transcription**

423 Synthetic DNA was purchased from IDT that encoded a T7 promoter (TAATACGACTCACTATAGG), the hu-  
424 man  $\beta$ -globin 5' UTR, a nanoLuciferase ORF, and the human  $\beta$ -globin 3' UTR, with a boxB motif (GCCCT-  
425 GAAGAAGGGC) either inserted or not. This was amplified with Phusion High-Fidelity DNA polymerase (Ther-  
426 moFisher, cat # F530S) and primers CPL\_184 and CPL\_262. The PCR product was purified using a PureLink  
427 Quick PCR Purification Kit (Invitrogen, cat # K310002). After amplification, the RNAs were *in vitro* transcribed  
428 using a MEGAscript T7 Transcription Kit (ThermoFisher, cat # AM1334) for 3 hours at 37 °C and treated with Turbo  
429 DNase for 15 minutes at 37 °C. Transcribed RNA was purified via a GeneJET RNA Purification kit (ThermoSci-  
430 entific, cat # K7032), followed by Micro Bio-Spin P-6 Gel Columns (Bio-Rad, cat # 7326221) equilibrated 3x with  
431 200  $\mu$ L of water. The purity of RNA was determined by agarose gel electrophoresis and quantified by Nanodrop.

## 432 **Low throughput RNA editing assay**

433 The reporter mRNAs (125 nM each, containing either boxB or not) were refolded in water by heating to 95 °C  
434 for 2 minutes and then cooled slowly to RT. The refolded mRNAs were added to a reaction mixture containing  
435 TadA buffer (50 mM Tris-HCl pH 7.5, 25 mM KCl, 2 mM MgCl<sub>2</sub>). After incubating at 37 °C for 5 minutes, the  
436 indicated TadA recombinant protein (250 nM) was added. For nanobody and antibody recruitment, 200 nM and  
437 100 nM of each reporter mRNA was used, respectively. Reactions were incubated at 37 °C for 2 hours. RNA  
438 was purified via a GeneJET RNA purification kit and quantified by Nanodrop. Purified RNA (375 ng) and DNA  
439 primer CPL\_372 (1  $\mu$ M) were incubated together at 65 °C for 5 minutes and annealed on ice. RNA was reverse  
440 transcribed using Maxima RT (ThermoFisher, cat # EP0742) at 50 °C for 30 minutes followed by 85 °C for 5  
441 minutes. The resulting cDNA was amplified by PCR as described above using primers CPL\_373 and CPL\_374.  
442 The PCR products were purified and analyzed by nanopore sequencing (Plasmidsaurus). FASTQ files containing  
443 basecalled nanopore reads were sorted into populations that either contained the boxB element or did not. In both  
444 populations, the 40 nucleotides immediately 3' of the boxB motif insertion were compared against the non-edited  
445 reference sequence to identify adenosine to guanosine substitutions. Sequences with inserts or deletions were  
446 discarded. To determine the reported 95% confidence intervals, a bootstrapping analysis using rflip() from the  
447 mosaic package in R was used, with 100,000 iterations.

## 448 **BoxB reporter oligo library design**

449 Oligos for cloning the *in vitro* reporter pool were designed using a custom R script `design_invitro_oligo_pool.R`  
450 to generate a comprehensive library of sequence variants. Each oligo was composed of a 5' T7 promoter  
451 (TAATACGACTCACTATAGG), a forward handle (TGGCTTCGTTGTTGTGCT), a variable spacer region (TTTGT-  
452 GTTCTCTTGTTCGTTCTGGTTCGTT), a recorder region (TAGAATTACACCATAAT), and the boxB stem loop  
453 (GGGCCCTGAAGAAGGGCCC), with additional short buffer sequences flanking the variable regions. Barcode  
454 sequences devoid of A and separated by a Hamming distance of 2 were used to uniquely tag every oligo. To  
455 generate spacer variants, the full-length spacer sequence was truncated in two-nucleotide increments, creating  
456 a set of fragments; for each truncation, the spacer was split into 5' and 3' segments, and the fixed recorder  
457 region was inserted between these fragments to form a "spacer target" sequence. For randomizing the recorder  
458 region, all non-A nucleotides within the recorder were independently randomized in groups of 5 nucleotides to  
459 yield two distinct sets of target sequences. Each randomized spacer target was then incorporated into two oligo  
460 orientations by appending the boxB stem loop together with its buffer on either the 5' or the 3' side. The boxB  
461 stem loop was randomized in 3 or nt increments. The final oligo sequences are assembled by concatenating the  
462 T7 promoter, the forward handle, the designed variable region (incorporating spacer, recorder region, and boxB  
463 stem loops with their buffers), the barcode buffer with the assigned barcode, and a reverse transcription handle  
464 (GCTGGCTTCTGTTCCGTTTG). This oligo pool was ordered from IDT as oPool oAS2176. See Supplementary  
465 Table 4 for the full list.

466 Oligos for the *in vivo* reporter pool with randomized boxB stem loops were designed as above and ordered  
467 from IDT as oPool oRB262. See Supplementary Table 5 for full list.

468 Oligos for the  $\lambda$ N site saturation mutagenesis library were designed by replacing each codon in the  $\lambda$ N ORF  
469 by NNN. The oligos were ordered from IDT as oPool oRB275. See Supplementary Table 6 for full list.

#### 470 **High throughput *in vitro* RNA editing assay**

471 CPL\_303 (10  $\mu$ M) was pre-annealed to the oligo pool oAS2176 (10  $\mu$ M) in annealing buffer (20 mM Hepes  
472 pH 7.5, 100 mM KCl, and 2 mM MgCl<sub>2</sub>) by heating to 70 °C then cooling by 0.2 °C/s. The pool was transcribed  
473 and treated with DNase as described above. RNA was purified by phenol:chloroform extraction and ethanol  
474 precipitation.

475 The RNA libraries (250 nM total concentration) were added to TadA buffer along with any non-TadA fused  
476 protein (125, 250, or 500 nM). After incubating at 37 °C for 5 minutes, the indicated TadA recombinant protein was  
477 added equimolar to any non-TadA protein present. If the reaction contained the anti-GFP antibody, it was instead  
478 incubated for 1 hour at room temperature before TadA recombinant protein addition as previously described (Xiao  
479 et al. 2024a). The reactions were incubated at either 37 °C for 0.5, 1, or 2 hours, or 25 °C or 13 °C for 2 hours.  
480 RNA was purified by phenol:chloroform extraction and ethanol precipitation.

#### 481 **Cell culture**

482 HEK293T cells were cultured in Dulbecco's modified Eagle medium (DMEM 1X, with 4.5 g/L D-glucose, + L-  
483 glutamine, - sodium pyruvate, Gibco 11965-092) supplemented with 10% FBS (Thermo 26140079) and passaged  
484 using 0.25% trypsin in EDTA (Gibco 25200-056). Cells were grown at 37 °C in 5% CO<sub>2</sub>. Cell lines were confirmed  
485 to be free of mycoplasma contamination.

#### 486 **Integration of plasmid libraries into landing pad cell lines**

487 hsAS126.3 (HEK293T *attP\** *Cas9*) cells (Nugent et al. 2024) were seeded to 80% confluency in one 10 cm  
488 dish per library. 9.6  $\mu$ g of *attB\**-containing reporter library plasmid (pAS475, pAS476, and pAS517) and 2.4  $\mu$ g of  
489 Bxb1 expression vector (pAS344) were transfected per 10 cm dish using FuGENE HD reagent (Promega). Each  
490 library was transfected into a single 10 cm dish then expanded into 15 cm dishes 48 hours post-transfection. Cells  
491 were selected with 2  $\mu$ g/ml puromycin, added 72 hours post-transfection. Puromycin selection was ended after  
492 8 days, and cell pools were contracted back into a 10 cm dish. 24h after ending puromycin selection, 2  $\mu$ g/ml  
493 doxycycline was added to induce TadA and boxB library reporter expression.

#### 494 **Library mRNA extraction**

495 Library mRNA was harvested after 72 hr of doxycycline induction of TadA and boxB reporters from one 50-75%  
496 confluent 10 cm dish. Each 10 cm dish was treated with 1 ml .025% Trypsin, and neutralized with 5 mL DMEM  
497 media. Cells were pelleted from 1/3 of this cell suspension and resuspended in 1 ml Trizol reagent (Thermo).  
498 Total RNA from these lysates was then extracted using the Direct-zol RNA Miniprep kit (Zymo) following the  
499 manufacturer's protocol.

#### 500 **High throughput sequencing of boxB reporters**

501 2.3-7  $\mu$ g of total RNA from *in vivo* libraries or 25-200 ng RNA from each *in vitro* enzymatic reaction was reverse  
502 transcribed into cDNA using Maxima H Minus reverse transcriptase (Thermo) and RT primer oRB213 which also  
503 contains a 7 nt UMI. A 20-50  $\mu$ l PCR was performed using Phusion polymerase (Thermo) for 6-22 cycles with  
504 cDNA template comprising 1/20th of the final volume, and with oPN776 as the reverse primer. Indexed forward  
505 primers were used to enable pooled sequencing of all samples (one of oRB218-oRB225 or oRB287-oRB302).  
506 All PCR reactions generated a 192 bp amplicon that was cut out from a 2% agarose gel and cleaned using the  
507 Zymoclean Gel DNA Recovery Kit (Zymo). Libraries were sequenced on an Illumina NextSeq 2000 using custom  
508 sequencing primers. Custom primers were oRB214 for Read 1 (79 bp read), oRB215 for Read 2 (7bp read), and

509 oRB217 for indexing (7bp read).

## 510 **Computational analyses**

511 Pre-processing steps for high-throughput sequencing were implemented as Snakemake (Köster and Rahmann  
512 2012) workflows run within Singularity containers on an HPC cluster. All container images used in this study are  
513 publicly available as Docker images at <https://github.com/orgs/rasilab/packages>. Python (v3.9.15) and R (v4.2.2)  
514 programming languages were used for all analyses unless mentioned otherwise.

## 515 **Edited base counting for each boxB reporter variable region insert**

516 The raw data from boxB reporter sequencing are in FASTQ format. The boxB reporter oligo pool sequences  
517 was used to create a reference annotations file called `barcode_annotations.csv` containing 10-nt barcodes iden-  
518 tifying the locations of the A-Rich recorder region and variable region within the reporter sequence read. The  
519 10 nt barcode of each read was extracted and used to assign the entire read to an individual FASTQ file for each  
520 barcode in the `split_by_barcode.awk` script. The `calculate_summary_stats.ipynb` script then filtered reads  
521 to determine whether invariant sequences upstream and downstream of the A-rich reporter region match those  
522 documented in `barcode_annotations.csv` for that barcode. If a read passed the above filters, the A-rich recorder  
523 region, variable insert region, and UMI from each read was extracted according the start and length parameters  
524 for that barcode file referenced in `barcode_annotations.csv`. Only the first instance of each UMI was tallied.

525 For each unique combination of variable region, the total UMI count was tallied, as well as the the number  
526 of A,C,T and G reads for each of the 8 adenosine sites within the A-rich target region. Additionally, the number  
527 of reads with 0,1,2...8 total A,T,C and Gs were tallied for unique insert. The final list of insert, UMI and recorder  
528 region adenosine counts was printed as a `.csv` file for each boxB reporter barcode. These `.csv` files for each  
529 boxB reporter barcode were concatenated into one `.csv` table per condition for subsequence analysis using the  
530 `combine_barcode_summary_stats.ipynb` script.

## 531 **Statistical Methods**

532 For comparing GNRNA BoxB motifs: BoxB sequence variants were filtered to include only those for which  
533 >200 UMIs were detected, and maintained the closing U-A base pair at boxB positions 7 & 13.

534 Stem variants: Mean percent of reads with one or more adenine-to-guanine transitions observed in the  
535 recorder region was calculated for each stem loop variant across n=4 technical replicates. Each stem variant  
536 was assigned to percentile of free energy distribution based on Gibbs free energy calculated by RNAFold (see  
537 Figure 2I), such that each distribution represents n=50 or 51 stem variants.

538 DMS: The bootstrapped mean percentage of reads with 1+ base edits was calculated for each peptide variant  
539 and normalized to the bootstrapped mean for wild-type  $\lambda$ N.

## Figures

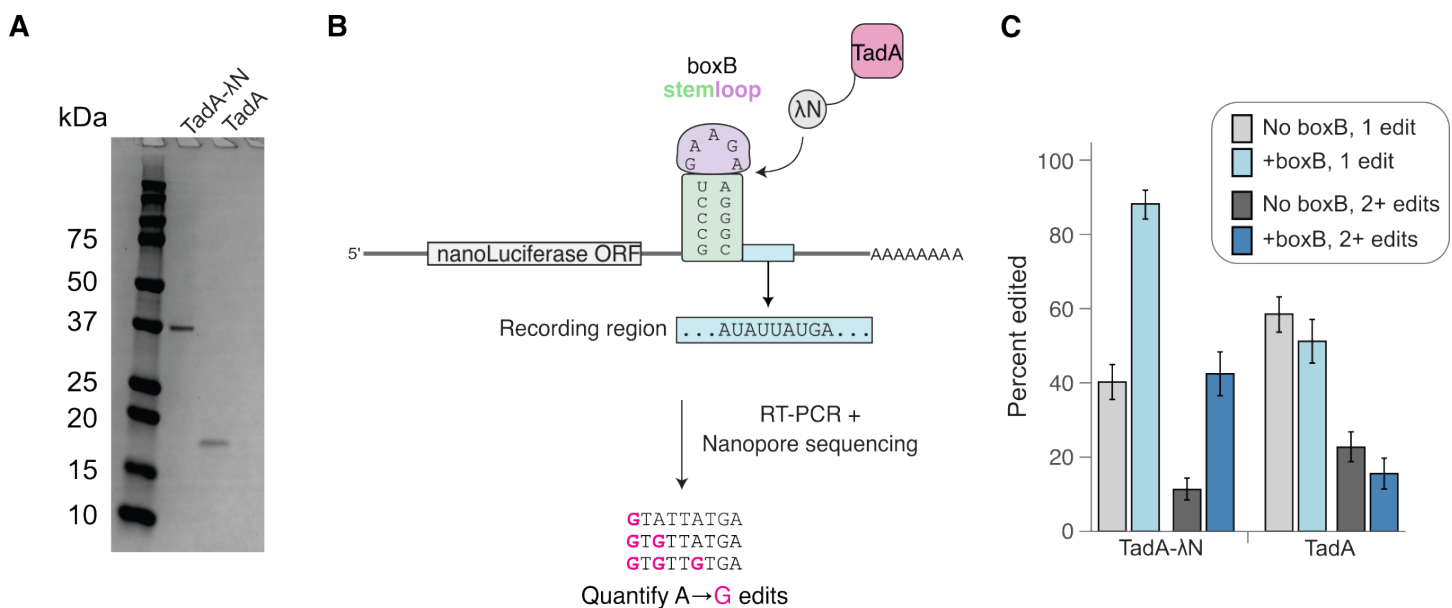


**Figure 1: TadA-λN specifically modifies boxB reporter RNA.**

**A.** SDS-PAGE of purified TadA-λN and free TadA8.20. Proteins visualized with Coomassie stain.

**B.** Schematic of boxB stem loop reporter and sequencing strategy to detect A-to-I edits. Control RNA reporters without boxB stem loop are not shown. Elements are not drawn to scale.

**C.** Editing efficiency of *in vitro* transcribed reporter RNAs incubated with TadA or TadA-λN. Error bars are 95% confidence intervals as determined by a binomial bootstrapping analysis.



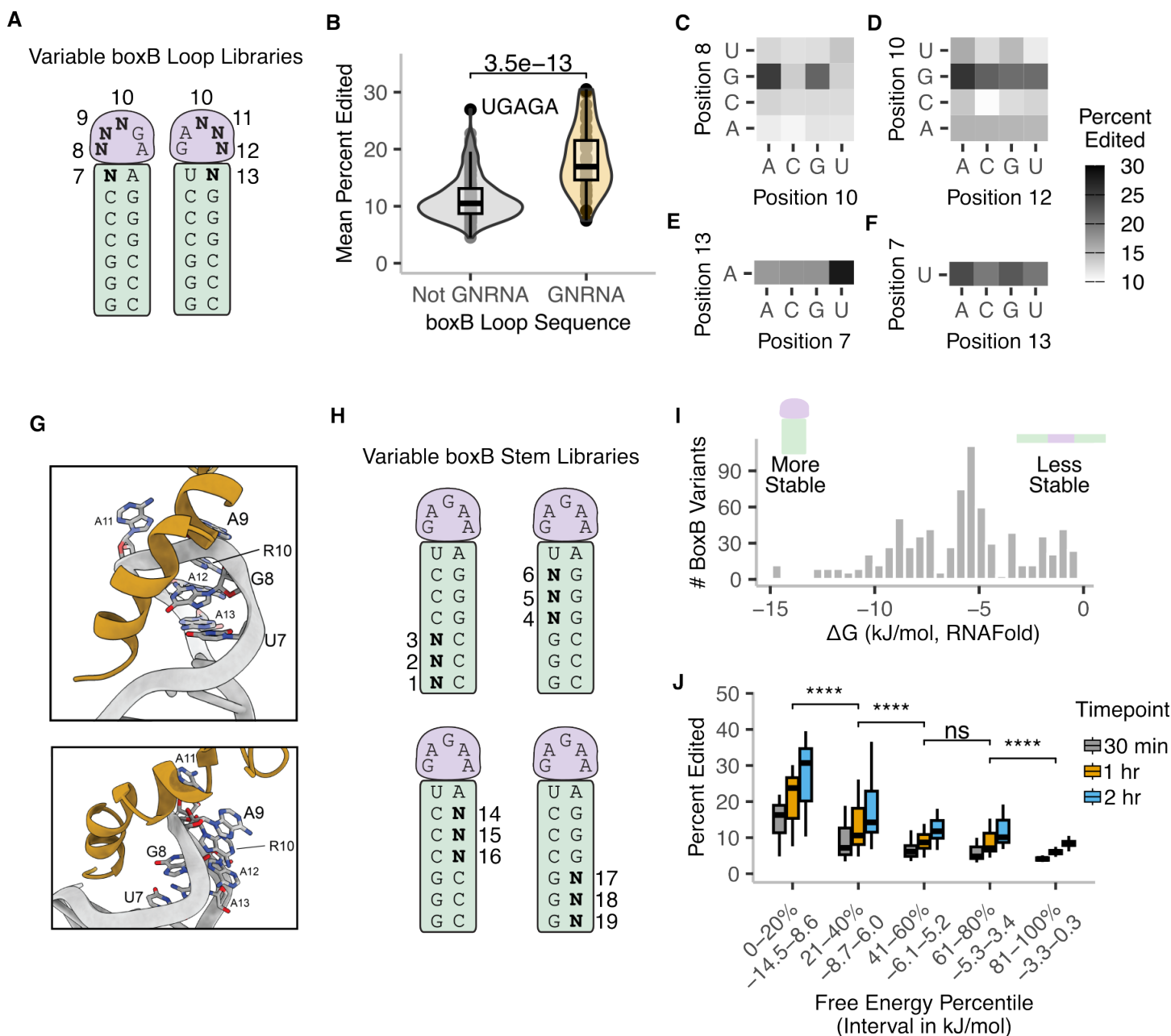


**Figure 3: TadA- $\lambda$ N editing quantitatively reflects RNA-RBP binding strength *in vitro*.**

**A.** boxB loop variant library design. N indicates a randomized base.

**B.** Mean editing efficiency of boxB loop variants with GNRNA motifs (n=41) to those without (n=223). Box plots indicate median and inter-quartile ranges. P-values calculated using two-sided Wilcoxon test.

**C-F.** Mean editing efficiency as a function of nucleotide at location 8 and 10 (C), 10 and 12 (D), 7 (E), 13 (F) of the boxB loop.

**G.** NMR structure of  $\lambda$ N peptide boxB complex with labeled loop nucleotides (Schärf et al. 2000).  $\lambda$ N is colored gold.

**H.** boxB stem variant library design. N indicates a randomized base.

**I.** Distribution of estimated free energy of all boxB stem variants. Free energy was calculated using RNAFold within the ViennaRNA package (Lorenz et al. 2011).

**J.** Mean editing efficiency of boxB stem variants. The 256 boxB stem variants were divided into 5 quintiles. Box plots indicate median and inter-quartile ranges. P-values were calculated using two-sided Wilcoxon test. \*\*\*\* p < 0.0001, n.s. p > 0.05.

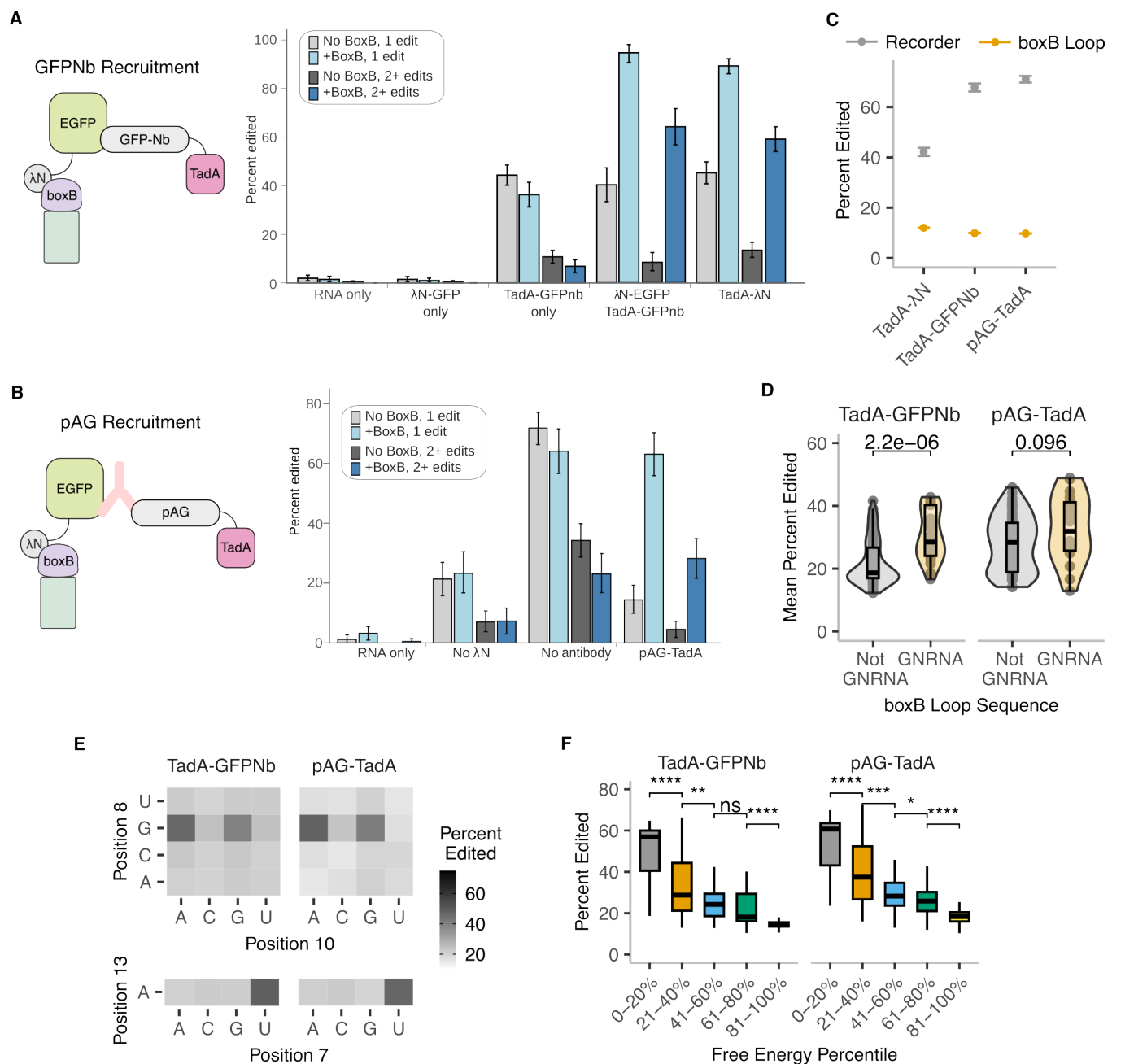


**Figure 4: Split recruitment of TadA and lambdaN preserves RNA editing specificity.**

**A.** (Left) Schematic of TadA-GFPNb recruitment strategy to boxB RNA reporters. (Right) Editing efficiency of *in vitro* transcribed nanoluciferase reporter RNAs incubated with indicated components (see diagram, Figure 1B). Error bars are 95% confidence intervals as determined by a binomial bootstrapping analysis.

**B.** (Left) Schematic of pAG-TadA recruitment strategy to boxB RNA reporters. (Right) Editing efficiency of *in vitro* transcribed nanoluciferase reporter RNAs incubated with indicated components (see diagram, Figure 1B). Error bars are 95% confidence intervals as determined by a binomial bootstrapping analysis.

**C.** Mean editing efficiency across different recruitment methods in either the recorder region (grey) or boxB loop (orange). Error bars represent standard error over n=64 technical replicates. TadA-lambdaN data same as Figure 2, included here for comparison.

**D.** Comparison of editing efficiency of boxB loop variants with GNRNA motifs (n=26 for TadA-GFPNb, n=18 for pAG-TadA) to those without (n=126 for TadA-GFPNb and n=61 for pAG-TadA). Box plots indicate median and inter-quartile ranges. P-values calculated using two-sided Wilcoxon test.

**E.** Mean editing efficiency as a function of nucleotide identity at location 8 and 10 (top), and base 7 (bottom) of the boxB loop.

**F.** Mean editing efficiency of boxB stem variants. Free energy intervals are identical to those indicated in Figure 2J x-axis. Box plots indicate median and inter-quartile ranges. P-values were calculated using two-sided Wilcoxon test. \*\*\*\* p < 0.0001, \*\*\* p < 0.001, \*\* p < 0.01, \* p < 0.05, n.s p > 0.05.

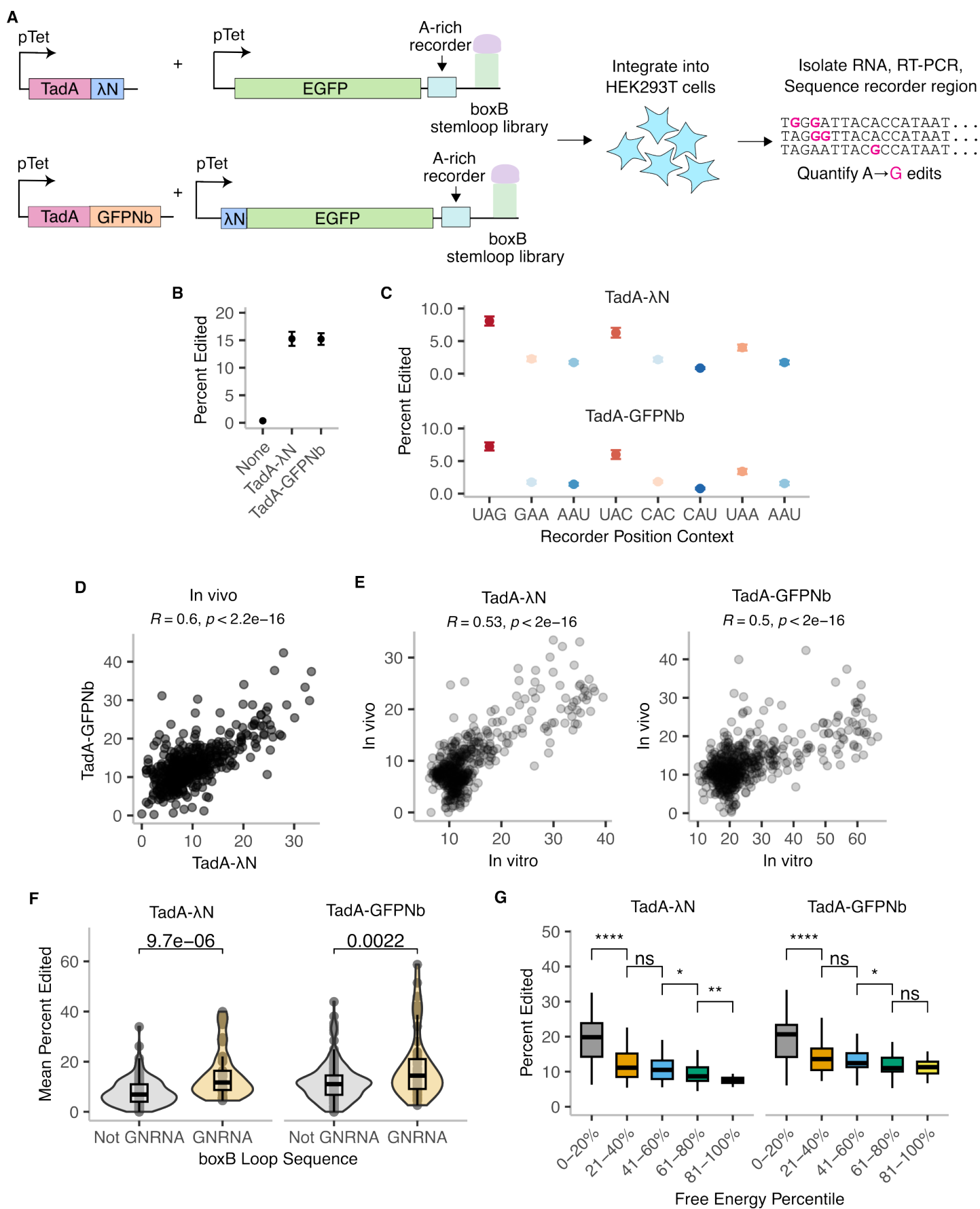


**Figure 5: *In vivo* TadA-λN editing reflects binding strength and context preferences.**  
(caption on next page)

(continued from previous page)

- A.** Schematic of TadA and boxB libraries design and integration into HEK293T cells. Elements not drawn to scale.
- B.** Mean editing efficiency in each *in vivo* library recorder region for wild-type BoxB reporters. Error bars represent standard error over n=24 technical replicates.
- C.** Mean editing efficiency at different adenines within the recorder region. Error bars denote standard error over 12 technical replicates.
- D.** Comparison of editing efficiency between TadA-GFPNb and TadA-λN *in vivo* for individual boxB variants. R represents Spearman correlation coefficient.
- E.** Comparison of editing efficiency between *in vitro* and *in vivo* for boxB variants in cells expressing TadA-λN or TadA-GFPNb. R represents Spearman correlation coefficient.
- F.** Comparison of editing efficiency of boxB loop variants with GNRNA motifs (n=33 for TadA-LN and n=42 for TadA-GFPNb) to those without (n= 141 for TadA-LN and n=208 for TadA-GFPNb). Box plots indicate median and inter-quartile ranges. P-values calculated using two-sided Wilcoxon test.
- G** Mean editing efficiency of boxB stem variants. Free energy intervals are identical to those indicated in Figure 2J x-axis. Box plots indicate median and inter-quartile ranges. P-values calculated using two-sided Wilcoxon test.
- \*\*\*\* p < 0.0001, \*\*\* p<0.001, \*\* p<0.01, \* p<0.05, n.s p > 0.05.

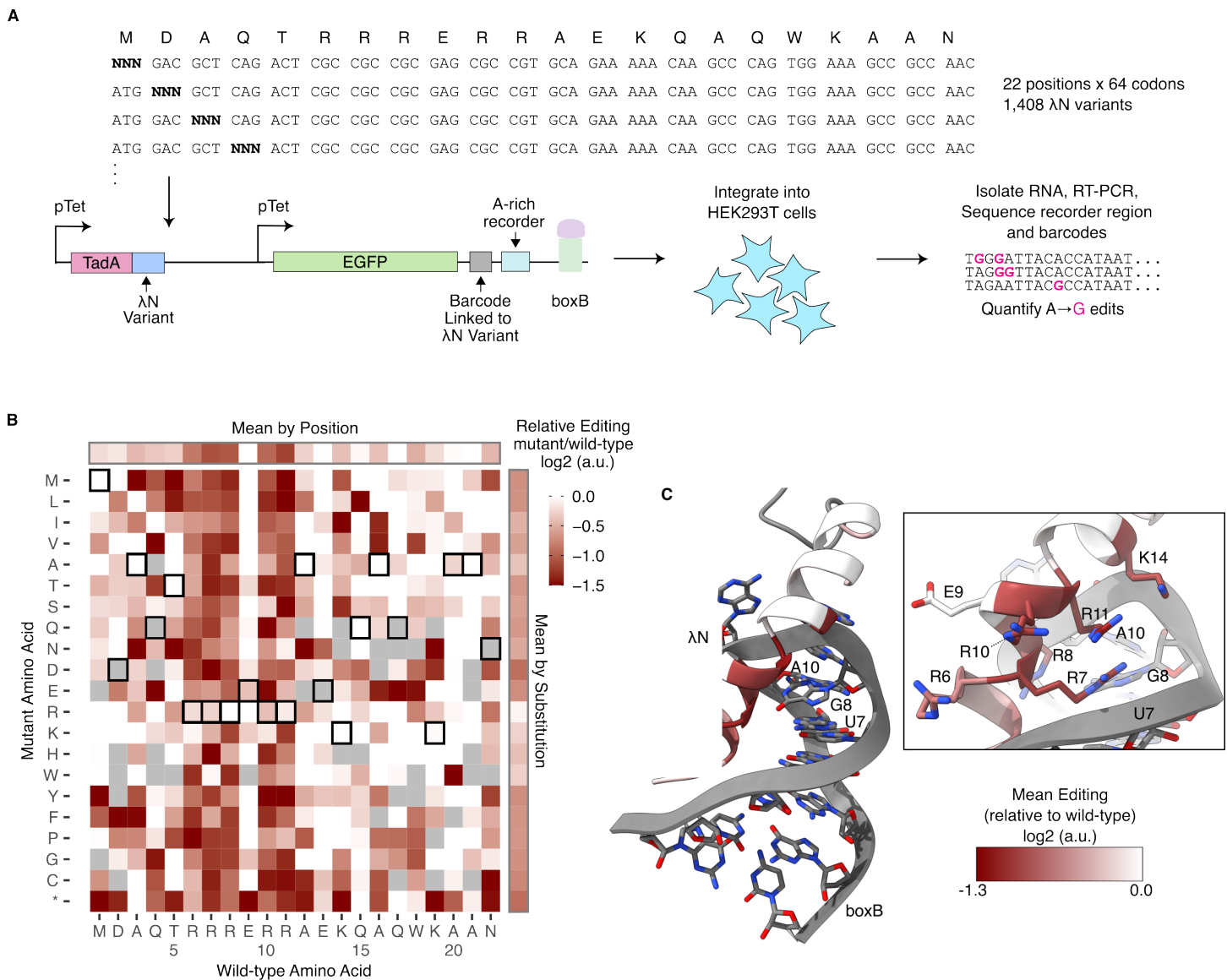


**Figure 6: Deep mutational scanning of  $\lambda$ N reveals key residues mediating RNA binding.**

**A.** Schematic of DMS library design and integration strategy into HEK293T cells. Elements not drawn to scale.

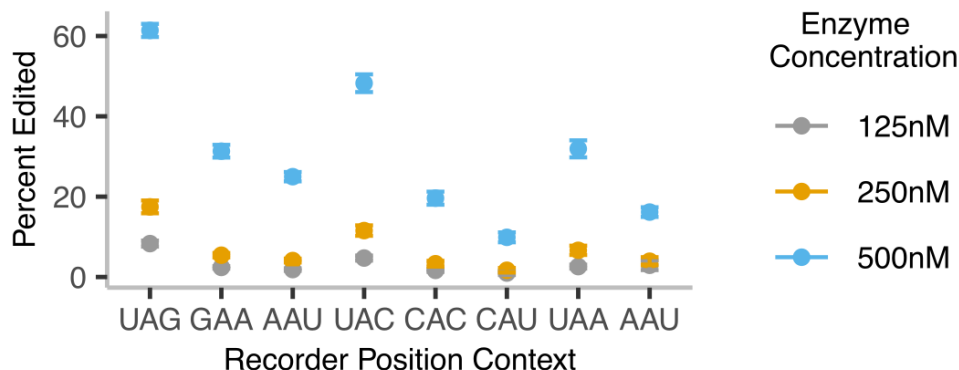
**B.** Relative editing efficiency of  $\lambda$ N variants as a function of residue position and identity. Log<sub>2</sub> ratios of mutant to wildtype are plotted from red (>1.5, loss of editing) to white (>0, neutral or gain of editing). Grey boxes indicates <3 barcodes were recovered for that amino acid variant.

Wild-type residues are indicated by a black outline.

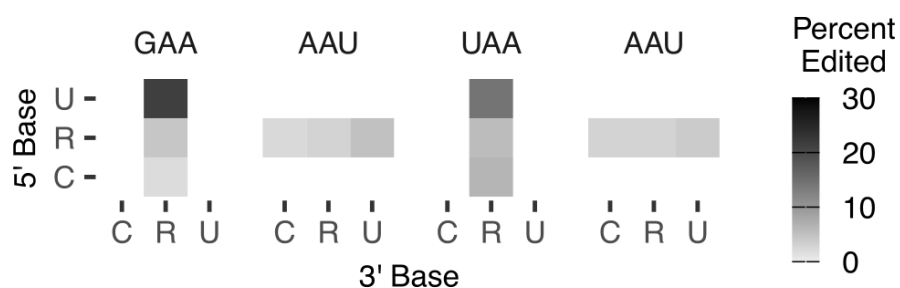
**C.** Per-residue log<sub>2</sub> ratio of normalized mean change in editing for nonsynonymous mutations mapped onto NMR structure for boxB-N peptide complex (Schärf et al. 2000).

## Supplementary Figures

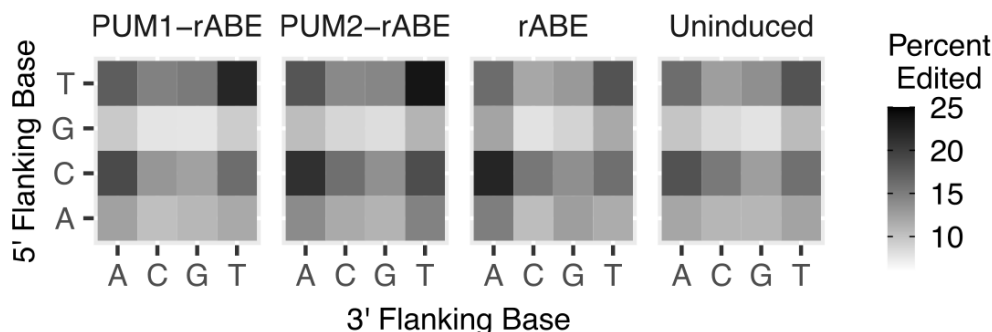
**A**



**B**



**C**

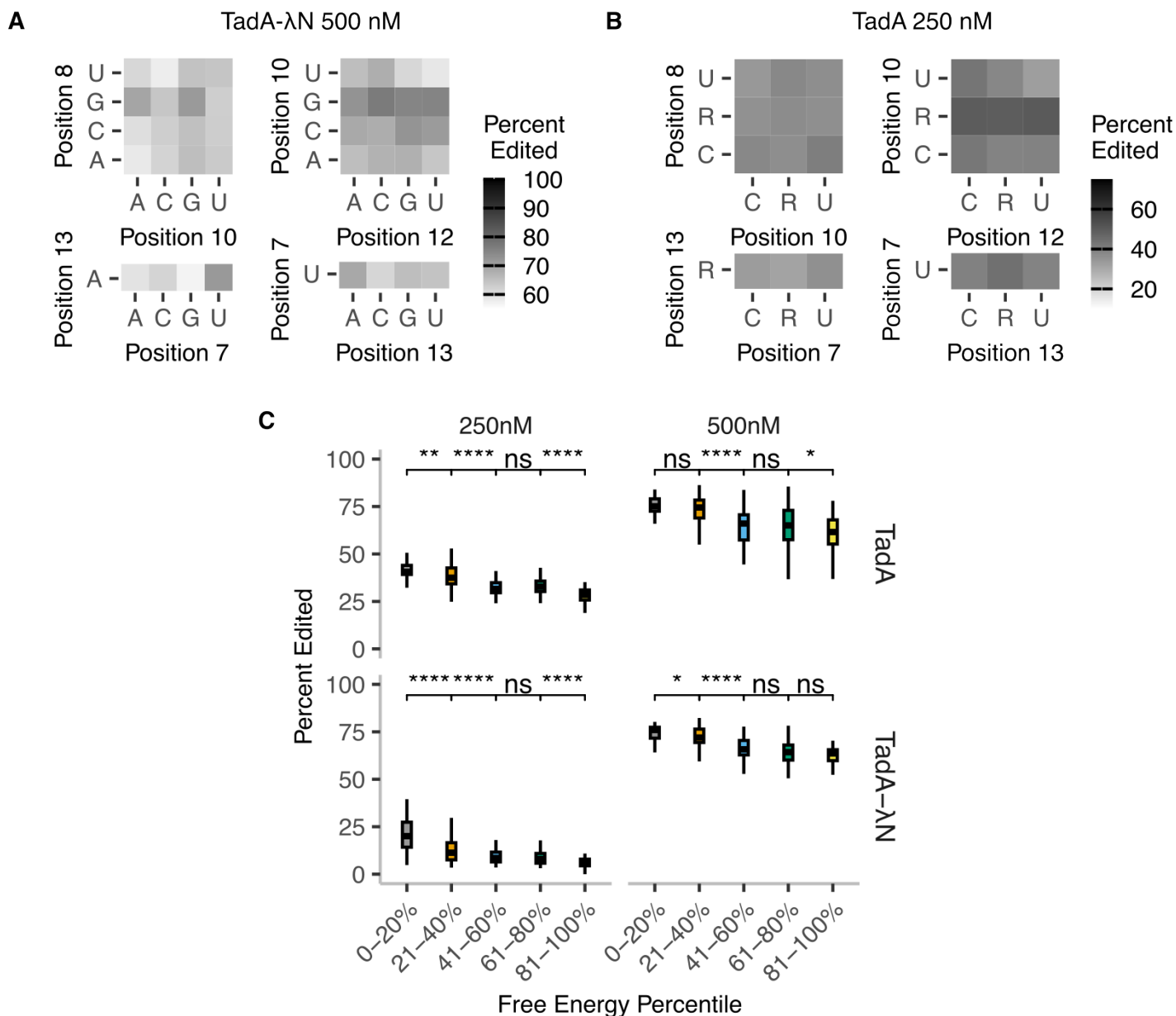


### Supplementary Figure 1: Analysis of TadA- $\lambda$ N editing.

**A.** Mean editing efficiency at different adenines within the recorder region for different concentrations of TadA- $\lambda$ N. Error bars denote standard error over 24 technical replicates.

**B.** Mean editing efficiency as a function of the nucleotide flanking the edited adenine. R represents G and A nucleotides, which were tallied together since we cannot resolve edited As from unedited Gs. Mean is calculated over 30 technical replicates.

**C.** Analysis of editing context dependence using RNA-Seq data from Lin et al (Lin et al. 2023). Heatmaps indicate mean percent of reads edited for all sites with the indicated 5' and 3' flanking bases. Only sites with at least 1 edited read and >10 total reads were included in this analysis.

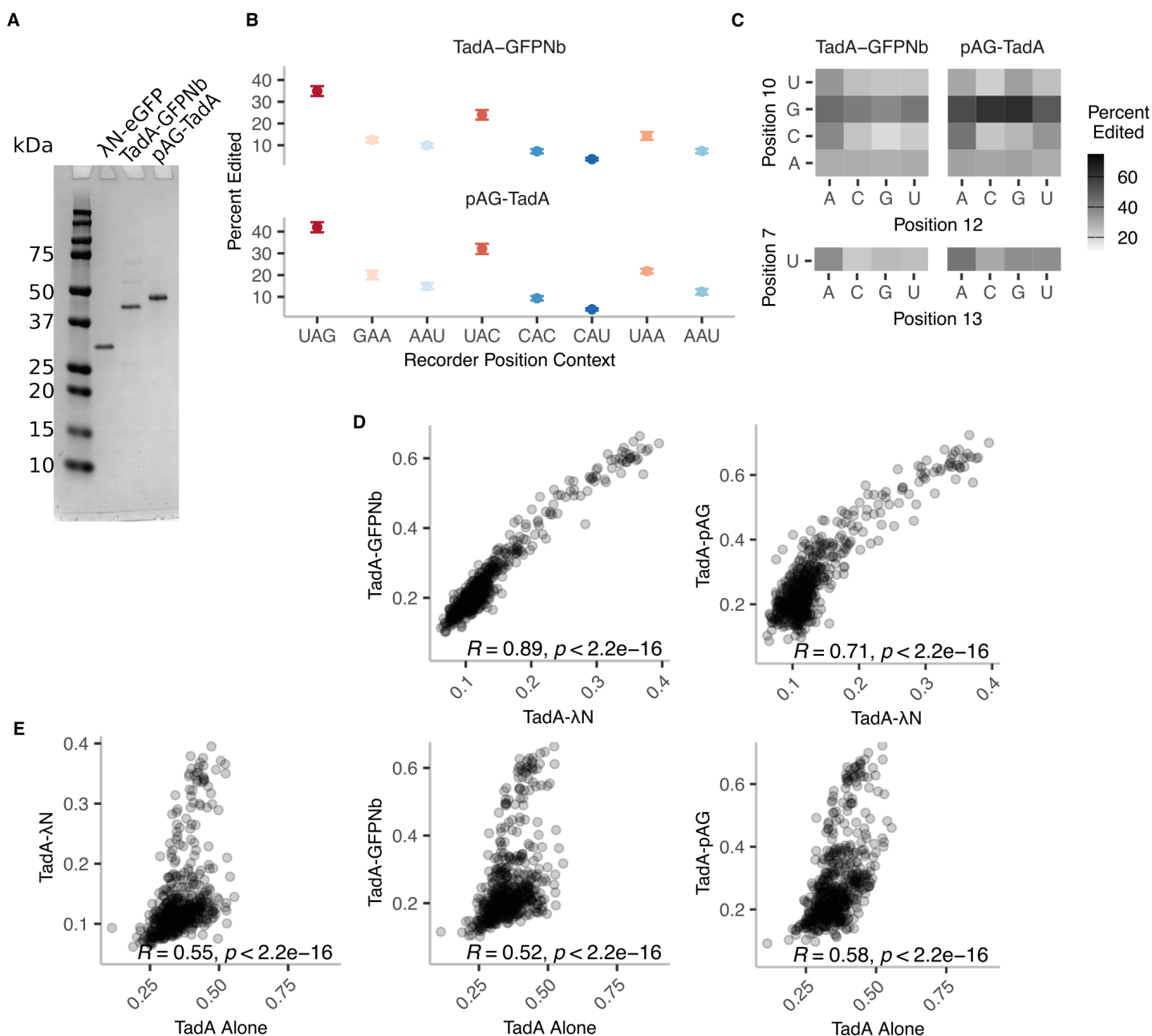


**Supplementary Figure 2: Analysis of TadA8.20 editing in nonspecific contexts.**

**A.** Mean editing efficiency as a function of nucleotide identity at location 8 and 10 (top-left heatmap), 10 and 12 (bottom-right) and base 7 and 13 (bottom heatmaps) of the boxB loop for TadA- $\lambda$ N fusion at 500nM Scales identical to those in Figure 3D-E for ease of comparison.

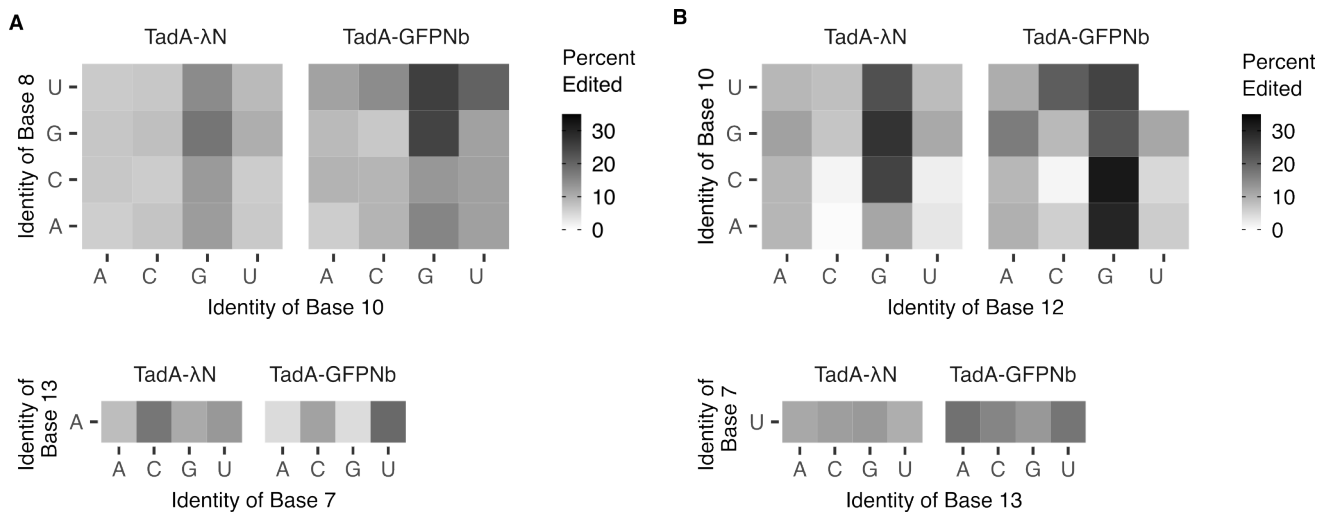
**B.** Mean editing efficiency as a function of nucleotide identity at location 8 and 10 (top-left heatmap), 10 and 12 (bottom-right) and base 7 and 13 (bottom heatmaps) of the boxB loop for TadA alone Scales identical to those in Figure 3D-E for ease of comparison. R represents G and A bases, which cannot be resolved due to the high rate of TadA editing in the boxB loop (Figure 2C).

**C** Mean editing efficiency of boxB stem variants for TadA- $\lambda$ N and TadA alone at 250nM and 500 nM. Free energy intervals are identical to those indicated in Figure 2J x-axis. Box plots indicate median and inter-quartile ranges. P-values were calculated using two-sided Wilcoxon test. \*\*\*\*  $p < 0.0001$ , \*\*\*  $p < 0.001$ , \*\*  $p < 0.01$ , \*  $p < 0.05$ , n.s  $p > 0.05$ .



### Supplementary Figure 3: Analysis of TadA recruitment strategies.

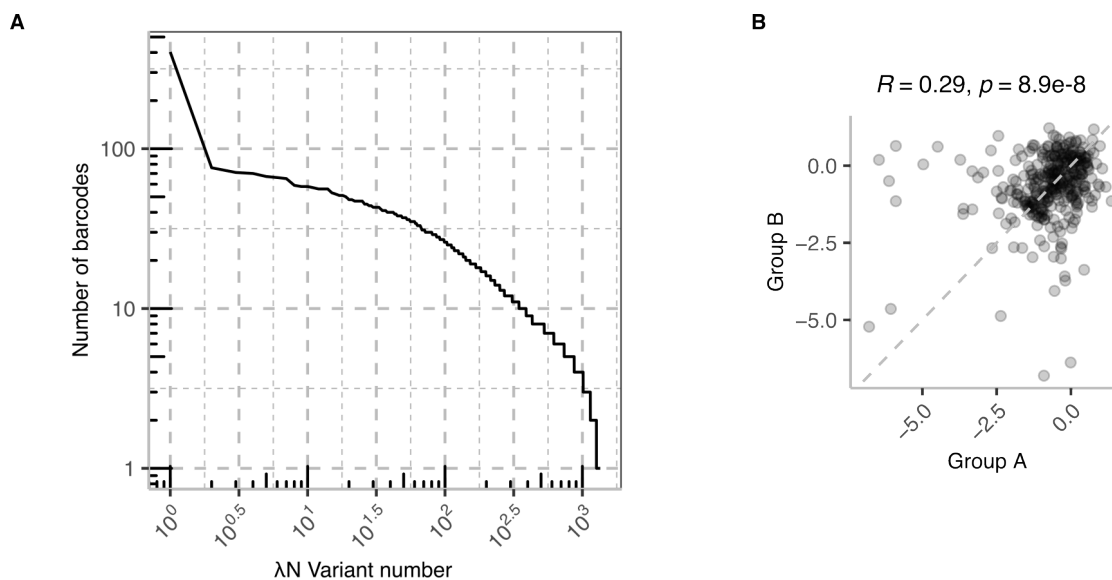
- A.** SDS-PAGE analysis of purified  $\lambda$ N-eGFP, TadA-GFPNb and pAG-TadA. Proteins visualized with Coomassie stain.
- B.** Quantification of editing of individual adenines within the recorder region for TadA-GFPNb (top panel) and pAG-TadA (bottom panel). Each point represents mean percentage of reads with an adenine-to-guanine transition observed at that position. The mean was calculated from each of  $n=24$  independent reporter libraries where reporter sequence was constant. Error bars represent standard error of the mean.
- C.** Mean editing efficiency as a function of nucleotide identity at location 10 and 12 (top heatmap) and 13 (bottom heatmaps) of the boxB loop for TadA alone. Scales identical to those in Figure 5E for comparison.
- D.** Comparison of editing efficiency between TadA-GFPNb and TadA- $\lambda$ N (left) and pAG-TadA and TadA- $\lambda$ N (right).  $R$  is Spearman correlation coefficient.
- E.** Comparison of editing efficiency between TadA- $\lambda$ N (left), TadA-GFPNb (middle), pAG-TadA (right) and TadA8.20 alone.  $R$  is Spearman correlation coefficient.



**Supplementary Figure 4: Analysis of *in vivo* TadA-λN and TadA-GFPNb editing.**

**A.** Mean editing efficiency as a function of nucleotide identity at location 8 and 10 (top heatmap) and 7 (bottom heatmaps) of the boxB loop for TadA alone. Scales identical to those in Figure 6 for comparison.

**B.** Mean editing efficiency as a function of nucleotide identity at location 10 and 12 (top heatmap) and 13 (bottom heatmaps) of the boxB loop for TadA alone. Scales identical to those in Figure 6 for comparison.



**Supplementary Figure 5: Analysis of  $\lambda$ N mutational scanning.**

**A.** Linked barcodes per unique  $\lambda$ N sequence variant. Unique 20nt barcodes were assigned to  $\lambda$ N sequence variants via deep sequencing of the plasmid pool. Sequence variants were arranged by number of barcodes assigned and given a number, plotted on the x-axis. The number of linked barcodes is plotted on the y-axis. The “Wild-type”  $\lambda$ N occurred at 22x times frequency in the plasmid pool and thus has a large number of barcodes assigned to it compared to all other sequences.

**B.** Correlation between barcode sets. For each  $\lambda$ N amino acid variant, individual linked barcodes were randomly partitioned into two sets, (or to within a barcode for odd number of detected barcodes). R refers to Spearman correlation coefficient between barcode groups.

## References

- Baron-Benhamou J, Gehring NH, Kulozik AE, Hentze MW. 2004. [Using the lambdaN peptide to tether proteins to RNAs](#). *Methods Mol Biol* **257**: 135–154.
- Becker WR, Jarmoskaite I, Vaidyanathan PP, Greenleaf WJ, Herschlag D. 2019. [Demonstration of protein cooperativity mediated by RNA structure using the human protein PUM2](#). *RNA* **25**: 702–712.
- Brannan KW, Chaim IA, Marina RJ, Yee BA, Kofman ER, Lorenz DA, Jagannatha P, Dong KD, Madrigal AA, Underwood JG, et al. 2021. [Robust single-cell discovery of RNA targets of RNA-binding proteins and ribosomes](#). *Nat Methods* **18**: 507–519.
- Chattopadhyay S, Garcia-Mena J, DeVito J, Wolska K, Das A. 1995. [Bipartite function of a small RNA hairpin in transcription antitermination in bacteriophage lambda](#). *Proceedings of the National Academy of Sciences* **92**: 4061–4065.
- De Gregorio E, Preiss T, Hentze MW. 1999. [Translation driven by an eIF4G core domain in vivo](#). *EMBO J* **18**: 4865–4874.
- Ellington AD, Szostak JW. 1990. [In vitro selection of RNA molecules that bind specific ligands](#). *Nature* **346**: 818–822.
- Gaudelli NM, Lam DK, Rees HA, Solá-Esteves NM, Barrera LA, Born DA, Edwards A, Gehrke JM, Lee S-J, Liquori AJ, et al. 2020. [Directed evolution of adenine base editors with increased activity and therapeutic application](#). *Nat Biotechnol* **38**: 892–900.
- Gebauer F, Schwarzl T, Valcárcel J, Hentze MW. 2021. [RNA-binding proteins in human genetic disease](#). *Nat Rev Genet* **22**: 185–198.
- Georgakopoulos-Soares I, Parada GE, Hemberg M. 2022. [Secondary structures in RNA synthesis, splicing and translation](#). *Computational and Structural Biotechnology Journal* **20**: 2871–2884.
- Jarmoskaite I, Denny SK, Vaidyanathan PP, Becker WR, Andreasson JOL, Layton CJ, Kappel K, Shivashankar V, Sreenivasan R, Das R, et al. 2019. [A Quantitative and Predictive Model for RNA Binding by Human Pumilio Proteins](#). *Mol Cell* **74**: 966–981.e18.
- Khyzha N, Henikoff S, Ahmad K. 2022. [Profiling RNA at chromatin targets in situ by antibody-targeted tagmentation](#). *Nat Methods* **19**: 1383–1392.
- Köster J, Rahmann S. 2012. [Snakemake—a scalable bioinformatics workflow engine](#). *Bioinformatics* **28**: 2520–2522.
- Lambert N, Robertson A, Jangi M, McGeary S, Sharp PA, Burge CB. 2014. [RNA Bind-n-Seq: quantitative assessment of the sequence and structural binding specificity of RNA binding proteins](#). *Mol Cell* **54**: 887–900.
- Lapointe CP, Wilinski D, Saunders HAJ, Wickens M. 2015. [Protein-RNA networks revealed through covalent RNA marks](#). *Nat Methods* **12**: 1163–1170.
- Legault P, Li J, Mogridge J, Kay LE, Greenblatt J. 1998. [NMR Structure of the Bacteriophage λ N Peptide/boxB RNA Complex: Recognition of a GNRA Fold by an Arginine-Rich Motif](#). *Cell* **93**: 289–299.
- Liang Q, Yu T, Kofman E, Jagannatha P, Rhine K, Yee BA, Corbett KD, Yeo GW. 2024. [High-sensitivity in situ capture of endogenous RNA-protein interactions in fixed cells and primary tissues](#). *Nat Commun* **15**: 7067.
- Lin Y, Kwok S, Hein AE, Thai BQ, Alabi Y, Ostrowski MS, Wu K, Floor SN. 2023. [RNA molecular recording with an engineered RNA deaminase](#). *Nat Methods* **20**: 1887–1899.
- Lorenz R, Bernhart SH, Höner zu Siederdissen C, Tafer H, Flamm C, Stadler PF, Hofacker IL. 2011. [ViennaRNA Package 2.0](#). *Algorithms for Molecular Biology* **6**: 26.

- Lou T-F, Weidmann CA, Killingsworth J, Hall TMT, Goldstrohm AC, Campbell ZT. 2017. [Integrated analysis of RNA-binding protein complexes using in vitro selection and high-throughput sequencing and sequence specificity landscapes \(SEQRS\)](#). *Methods* **118-119**: 171–181.
- McMahon AC, Rahman R, Jin H, Shen JL, Fieldsend A, Luo W, Rosbash M. 2016. [TRIBES: Hijacking an RNA-Editing Enzyme to Identify Cell-Specific Targets of RNA-Binding Proteins](#). *Cell* **165**: 742–753.
- Medina-Munoz HC, Kofman E, Jagannatha P, Boyle EA, Yu T, Jones KL, Mueller JR, Lykins GD, Doudna AT, Park SS, et al. 2024. [Expanded palette of RNA base editors for comprehensive RBP-RNA interactome studies](#). *Nat Commun* **15**: 875.
- Melamed D, Young DL, Gamble CE, Miller CR, Fields S. 2013. [Deep mutational scanning of an RRM domain of the \*Saccharomyces cerevisiae\* poly\(A\)-binding protein](#). *RNA* **19**: 1537–1551.
- Meyer KD. 2019. [DART-seq: an antibody-free method for global m6A detection](#). *Nat Methods* **16**: 1275–1280.
- Nugent PJ, Park H, Wladyka CL, Chen KY, Bynum C, Quarterman G, Hsieh AC, Subramaniam AR. 2024. [Decoding RNA Metabolism by RNA-linked CRISPR Screening in Human Cells](#). 2024.07.25.605204.
- Rahman R, Xu W, Jin H, Rosbash M. 2018. [Identification of RNA-binding protein targets with HyperTRIBES](#). *Nat Protoc* **13**: 1829–1849.
- Schärf M, Sticht H, Schweimer K, Boehm M, Hoffmann S, Rösch P. 2000. [Antitermination in bacteriophage  \$\lambda\$](#) . *European Journal of Biochemistry* **267**: 2397–2408.
- SenGupta DJ, Zhang B, Kraemer B, Pochart P, Fields S, Wickens M. 1996. [A three-hybrid system to detect RNA-protein interactions in vivo](#). *Proc Natl Acad Sci U S A* **93**: 8496–8501.
- Tan R, Frankel AD. 1995. [Structural variety of arginine-rich RNA-binding peptides](#). *Proc Natl Acad Sci U S A* **92**: 5282–5286.
- Thapar R, Denmon AP, Nikonowicz EP. 2014. [Recognition Modes of RNA Tetraloops And Tetraloop-Like Motifs By RNA Binding Proteins](#). *Wiley Interdiscip Rev RNA* **5**: 10.1002/wrna.1196.
- Tuerk C, Gold L. 1990. [Systematic Evolution of Ligands by Exponential Enrichment: RNA Ligands to Bacteriophage T4 DNA Polymerase](#). *Science* **249**: 505–510.
- Ule J, Jensen K, Mele A, Darnell RB. 2005. [CLIP: a method for identifying protein-RNA interaction sites in living cells](#). *Methods* **37**: 376–386.
- Wolf J, Gerber AP, Keller W. 2002. [tadA, an essential tRNA-specific adenosine deaminase from \*Escherichia coli\*](#). *EMBO J* **21**: 3841–3851.
- Xiao Y, Chen Y-M, Zou Z, Ye C, Dou X, Wu J, Liu C, Liu S, Yan H, Wang P, et al. 2024a. [Profiling of RNA-binding protein binding sites by in situ reverse transcription-based sequencing](#). *Nat Methods* **21**: 247–258.
- Xiao Y-L, Liu S, Ge R, Wu Y, He C, Chen M, Tang W. 2023. [Transcriptome-wide profiling and quantification of N6-methyladenosine by enzyme-assisted adenosine deamination](#). *Nat Biotechnol* **41**: 993–1003.
- Xiao Y-L, Wu Y, Tang W. 2024b. [An adenine base editor variant expands context compatibility](#). *Nat Biotechnol* **42**: 1442–1453.
- Yarnall MTN, Ioannidi EI, Schmitt-Ulms C, Krajeski RN, Lim J, Villiger L, Zhou W, Jiang K, Garushyants SK, Roberts N, et al. 2023. [Drag-and-drop genome insertion of large sequences without double-strand DNA cleavage using CRISPR-directed integrases](#). *Nat Biotechnol* **41**: 500–512.
- Zhao J, Ohsumi TK, Kung JT, Ogawa Y, Grau DJ, Sarma K, Song JJ, Kingston RE, Borowsky M, Lee JT. 2010. [Genome-wide Identification of Polycomb-Associated RNAs by RIP-seq](#). *Molecular Cell* **40**: 939–953.